SEDIMENTOLOGY the journal of the International Association of Sedimentologists

Sedimentology (2017) **64**, 871–902 doi: 10.1111/sed.12336

Fine-grained agglutinated elongate columnar stromatolites: Tieling Formation, *ca* 1420 Ma, North China

FABIO TOSTI and ROBERT RIDING
Department of Earth and Planetary Sciences, University of Tennessee, Knoxville, TN 37996, USA (E-mail: rriding@utk.edu)

Associate Editor – Peir Pufahl

ABSTRACT

The Mesoproterozoic Tieling Formation, near Jixian, northern China, contains thick beds of vertically branched, laterally elongate, columnar stromatolites. Carbonate mud is the primary component of both the stromatolites and their intervening matrix. Mud abundance is attributed to water column 'whiting' precipitation stimulated by cyanobacterial photosynthesis. Neomorphic microspar gives the stromatolites a 'streaky' microfabric and small mud flakes are common in the matrix. The columns consist of low-relief, mainly non-enveloping, laminae that show erosive truncation and well-defined repetitive lamination. In plan view, the columns form disjunct elongate ridges <10 cm wide separated by narrow matrix-filled runnels. The stromatolite surfaces were initially cohesive, rather than rigid, and prone to scour, and are interpreted as current aligned microbial mats that trapped carbonate mud. The pervasive ridge–runnel system suggests scale-dependent biophysical feedback between: (i) carbonate mud supply; (ii) current duration, strength and direction; and (iii) growth and trapping by prolific mat growth. Together, these factors determined the size, morphology and arrangement of the stromatolite columns and their laminae, as well as their branching patterns, alignment and ridge–runnel spacing. Ridge–runnel surfaces resemble ripple mark patterns, but whether currents were parallel and/or normal to stromatolite alignment remains unclear. The formation and preservation of Tieling columns required plentiful supply of carbonate mud, mat-building microbes well-adapted to cope with this abundant sediment, and absence of both significant early lithification and bioturbation. These factors were time limited, and Tieling stromatolites closely resemble coeval examples in the Belt-Purcell Supergroup of Laurentia. The dynamic interactions between mat growth, currents and sediment supply that determined the shape of Tieling columns contributed to the morphotypical diversity that characterizes mid–late Proterozoic branched stromatolites.

Keywords Agglutinated, branching, China, elongation, lamination, Mesoproterozoic, microfabric, morphology, stromatolite.

INTRODUCTION

Stromatolites are laminated microbial sediments (Kalkowsky, 1908) produced by sediment trapping and/or carbonate precipitation in microbial mats (Awramik & Margulis, 1974; Burne & Moore, 1987). Present-day marine stromatolites were first recognized by Black (1933) who found low-relief domes of laminated fine-grained sediment trapped by cyanobacterial mats at Andros Island in the Bahamas. This discovery strongly influenced research by focusing attention on the importance of sediment trapping in stromatolite Formation (Young, 1934; Fenton & Fenton,

1937; Cloud & Barnes, 1948; Rezak, 1957). However, it was subsequently realized that during burial, these poorly lithified Andros deposits are disrupted by burrowing organisms (Shinn *et al.*, 1969). This led Garrett (1970) to suggest that cohesive, but essentially unlithified, fine-grained stromatolites such as those at Andros would only have been widespread in subtidal environments, and readily preserved into the rock record, prior to the appearance of animal life.

This study describes Mesoproterozoic stromatolites in the upper (*ca* 1·44 to 1·40 Ga) Tieling Formation of northern China that were formed by trapping fine-grained sediment: essentially, carbonate mud. Their laminae are well-preserved and they show no indications of bioturbation. Current estimates place amoebozoan, bikont and opisthokont origins at *ca* 1·0 Ga (Porter & Knoll, 2000; Berney & Pawlowski, 2006), followed by animals *ca* 800 Ma (Erwin *et al.*, 2011). Lack of bioturbation in *ca* 1·42 Ga Tieling stromatolites is therefore consistent with Garrett's (1970) prediction. Absence of meiofauna and macrofauna would have allowed mats to develop extensively and also to be preserved. In addition to conditions promoting their preservation, formation of Tieling stromatolites required abundant fine-grained allochthonous carbonate sediment. Widespread occurrence of carbonate mud in the upper Proterozoic has been attributed to increased water column precipitation ('whitings') (Knoll & Swett, 1990; Grotzinger, 1994), linked to changes in seawater carbonate chemistry that reduced sea floor precipitation, while increasing the importance of trapping in stromatolite Formation (Grotzinger & Knoll, 1999). This development may have been linked to progressive decline in atmospheric CO_2 that was sufficient to induce CO_2-concentrating mechanisms (CCM) in cyanobacteria and thereby promote marine whiting precipitation (Riding, 2006).

A widely noted, but possibly underappreciated, feature of Proterozoic columnar stromatolites is that they can be elongate in plan view. End-on, the examples described here are upright branched columns, *ca* 5 cm wide and up to 30 cm or more in height. In plan view, the same columns are elongate, up to 40 cm in length, and have wall-like geometry, mutually aligned, end to end and side by side; they form extensive beds of innumerable vertically packed slabs, mutually separated by vertical matrix-filled spaces. The tops of the elongate columns exposed on the sediment surface would have formed narrow ridges separated by the narrower matrix-filled runnels. The columns consist of well-defined laminae that cross-cut one another, show rapid lateral changes in thickness and had low synoptic relief; they appear to have been cohesive but not lithified during accretion. The columns show vertical fluctuations in width and frequent branching that reflect fluctuations in relative sediment accumulation rate. All of these features, together with those of the self-organized ridge–runnel system, suggest dynamic interaction between mat growth and copious current-borne sediment. The variety of morphotypes generated by these organo-sedimentary processes is mirrored in the taxonomic diversity of mid–late Proterozoic columnar stromatolites. These Tieling examples therefore shed light on fine-agglutinated stromatolite formation in mud-rich, animal-poor environments, and assist their wider recognition.

NORTH CHINA AND THE JIXIAN SECTION

The development of Proterozoic supercontinents, successively dominated by Kenorland (*ca* 2·7 to 2·0 Ga), Nuna/Columbia (*ca* 1·8 to 1·3 Ga) and Rodinia (*ca* 1·0 to 0·7 Ga) (Hoffman, 1989; Meert & Powell, 2001; Rogers & Santosh, 2002), continues to be explored (Ernst *et al.*, 2013; Evans, 2013; Roberts, 2013). This discussion includes the North China Craton (NCC), whose blocks and suture zones (Santosh *et al.*, 2010) are thought to have undergone final assembly following collision of Eastern and Western Archaean basement blocks at *ca* 1·85 Ga (Zhao, 2001). Late Palaeoproterozoic magmatic history of the region has been linked to both extensional rifting and further marginal accretion (Zhao & Cawood, 2012; Li *et al.*, 2013). Proterozoic sediments relevant to Nuna/Columbia and Rodinia history that postdate *ca* 1·85 Ga amalgamation of the North China Craton (Lu *et al.*, 2008), extend for hundreds of kilometres through the Yan Mountains (Yanshan), west and east of Beijing. These sediments underwent Permian–Cretaceous deformation (Zhang *et al.*, 2011) but numerous well-preserved areas have survived. One of the best known is the 'Jixian Section', a readily accessible region north of Jixian city, 90 km east of Beijing (Gao *et al.*, 1934; fig. 4; Chen *et al.*, 1980, 1981; Cao & Yuan, 2003; Chu *et al.*, 2007; Guo *et al.*, 2013; Shi *et al.*, 2014) (Fig. 1).

The Jixian Proterozoic succession overlies Archaean gneiss and schist near the Great Wall,

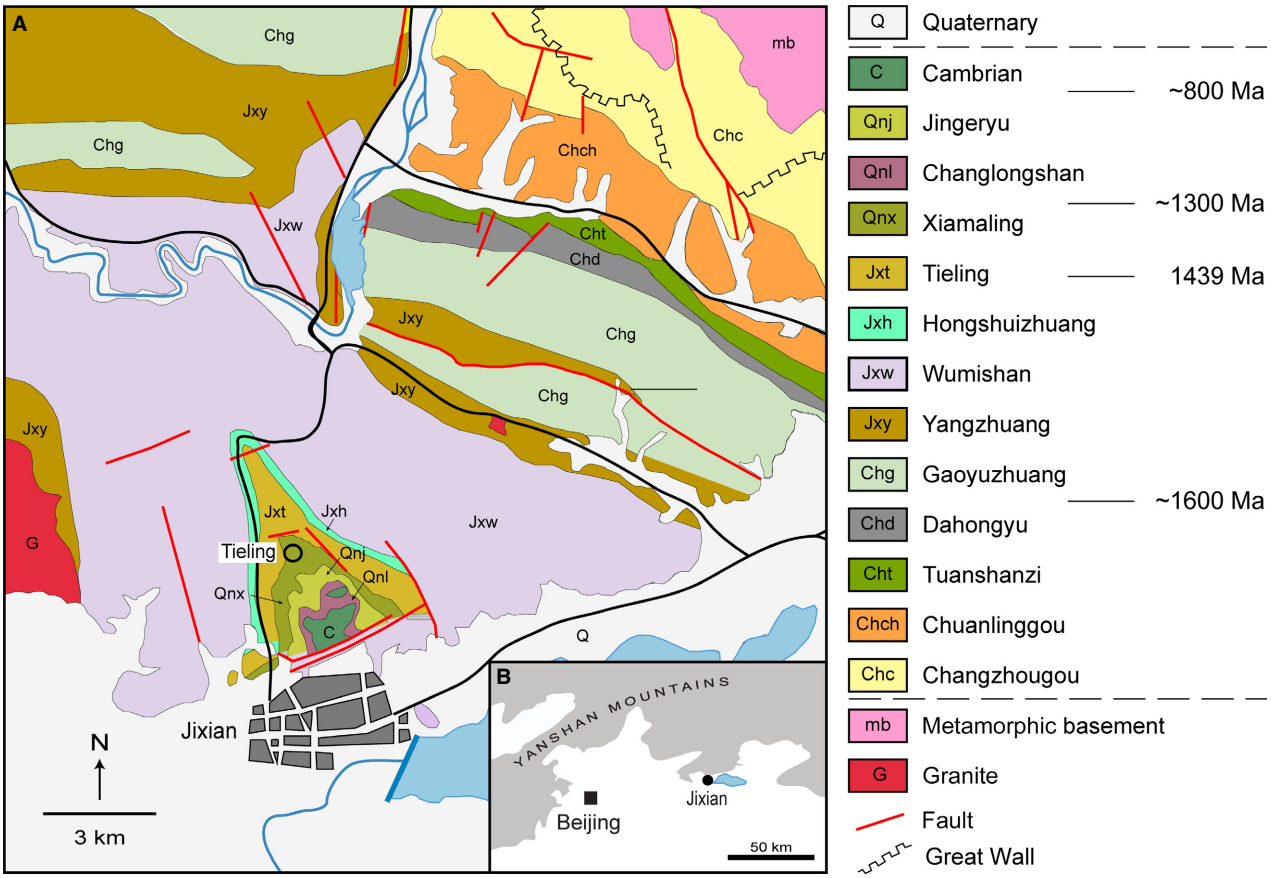

Fig. 1. (A) Location of Tieling village in the southern part of the classic 'Jixian section' of Proterozoic sediments, between Jixian city and the Great Wall. Immediately north of Jixian, the Tieling Formation (Jxt) crops out in a NNW–SSE trending syncline. From Su *et al.* (2010) and Li *et al.* (2013, 2014). (B) Location of Jixian, 90 km east of Beijing.

and extends south for *ca* 20 km to near Jixian city where it is overlain by Cambrian rocks. It consists of *ca* 9·5 km of siliciclastic and carbonate sediments, *ca* 1650 to 800 Myr in age. The lower part (*ca* 1650 to 1320 Ma) is generally divided into the Changcheng Group (Changzhougou, Chuanlinggou, Tuanshanzi and Dahongyu formations), the Jixian Group (Gaoyuzhuang, Yangzhuang, Wumishan, Hongshuizhuang and Tieling formations) and the Xiamaling Formation. The upper part (*ca* 1000 to 800 Ma) consists of the Qingbaikou Group (Changlongshan and Jingeryu formations) (Su *et al.*, 2010, fig. 6). These ages are based on SHRIMP dates (Gao *et al.*, 2007, 2008; Lu *et al.*, 2008; Li *et al.*, 2009, 2010; Su *et al.*, 2008, 2010; Li *et al.*, 2013, tables 1 and 2). The Changzhougou–Xiamaling succession as a whole was previously regarded as *ca* 1800 to 950 Ma, and the Jixian Group (with the Tieling Formation at its top) as *ca* 1400 to 1000 Ma (Chen *et al.*, 1981; Lu, 1992). The new dates suggest that the Changzhougou Group is Late Palaeoproterozoic, whereas the Jixian Group and Xiamaling Formation are *ca* 1600 Myr to *ca* 1320 Myr old (early to mid-Mesoproterozoic), and that the remainder of the Mesoproterozoic is absent (Li *et al.*, 2013, table 2).

The *ca* 1650 to 1400 Myr old Changcheng–Jixian succession, with the Tieling Formation at its top (Li *et al.*, 2013), is currently thought to have accumulated in an extensive ensialic basin, the Yanliao Aulacogen (Qian, 1985) on the Eastern Block of the NCC, as part of Nuna/Columbia (Zhai *et al.*, 2000; Zhao *et al.*, 2002, 2004; Lu *et al.*, 2008; Zhang *et al.*, 2012; Chen *et al.*, 2013; Li *et al.*, 2013; Qu *et al.*, 2014, fig. 2), prior to rifting and emplacement of diabase sills at *ca* 1·35 Ga that marks 'final breakup of the NCC from the Columbia supercontinent' (Zhao & Cawood, 2012; Zhao, 2014). These details assist interpretation of the position of the NCC within

Nuna/Columbia and subsequently in Rodinia (Bogdanova *et al.*, 2009; Pesonen *et al.*, 2012; Wilde, 2014). Recent global continental reconstructions have placed the NCC external to India and to portions of Australia on the south-east side of Nuna at *ca* 1·6 Ga (Zhang *et al.*, 2012), and external to Siberia and portions of Australia on the eastern side of Nuna at 1·45 Ga (Pisarevsky *et al.*, 2014). Chen *et al.* (2013) placed North China close to India and Siberia, and Wang *et al.* (2015) placed it between Laurentia and Baltica. Zhang *et al.* (2012, fig. 5b) proposed that from *ca* 1·80 to 1·4 Ma, North China was in an equatorial to low-latitude location, consistent with red beds, reefs (presumably the Tieling stromatolites) and dolomites in these deposits, and that the Jixian area was approximately 25 degrees north during Tieling deposition.

Much of the Changcheng Group and Jixian Group succession (*ca* 1650 to 1400 Ma) is dominated by carbonates (Su *et al.*, 2010; Meng *et al.*, 2011, fig. 3). Stromatolites are locally abundant, particularly in the Wumishan and Tieling formations of the Jixian Group. They include microdigitate forms (for example, *Pseudogymnosolen*) and large *Jacutophyton* in the Wumishan, and numerous columnar and branched forms (attributed to *Anabaria*, *Baicalia* and *Chihsienella*) in the Tieling (Cao & Yuan, 2003).

TIELING FORMATION AND STROMATOLITE UNIT

The stromatolites described here occur in the upper part of the Tieling Formation near Tieling village, *ca* 5 km north of Jixian city. Gao *et al.* (1934) described the Tieling Limestone in this area as about 350 m thick, comparatively pure and characterized by abundant *Collenia*. The Tieling Limestone was renamed the Tieling Formation during the First National Stratigraphic Congress of China in 1959 (see Su *et al.*, 2010). It occurs extensively in the Yanshan (Yan Mountains), from west of Beijing to east of Chengde – a distance of at least 400 km (Su *et al.*, 2010; Qu *et al.*, 2014, fig. 6). In its type area near Tieling, Chen *et al.* (1980) subdivided the formation into: (i) the lower Daizhuangzi Member (153 m of sandstone, shale, manganiferous dolostone, limestone, thin stromatolite bioherms); and (ii) the upper Laohuding Member (180 m of manganiferous dolomite and dolomitic limestone, overlain by a thick stromatolitic unit and then dolomitic limestone) (see Su *et al.*, 2010) (Fig. 2). Based on the Chen *et al.* (1980) overall thickness of 180 m for the Laohuding Member near Tieling village, the following subunits of this member are recognized here: (i) a lower non-stromatolitic unit, 93 m; (ii) an upper stromatolitic unit (here named the 'Stromatolite Unit'), 77 m; and (iii) a topmost non-stromatolitic unit, 10 m thick. In addition, the Stromatolite Unit is subdivided into three parts: lower 32 m, middle 13 m and upper 32 m (Fig. 2). The overlying Xiamaling Formation is regionally disconformable (and locally unconformable) on the Tieling Formation (Qu *et al.*, 2014, fig. 6).

Age

Based on zircons in a bentonite in the middle part of the formation, the Tieling Formation is currently dated 1437 ± 21 Ma, at Liujiagou, about 140 km north-east of Jixian (Su *et al.*, 2010) and 1439 ± 14 Ma at Dayu Shan, 4 km south of Tieling village (Li *et al.*, 2014). Based on these dates and an age of *ca* 1380 Ma for the overlying Xiamaling Formation at Liujiagou, Su *et al.* (2010) estimated *ca* 1·4 Ga as

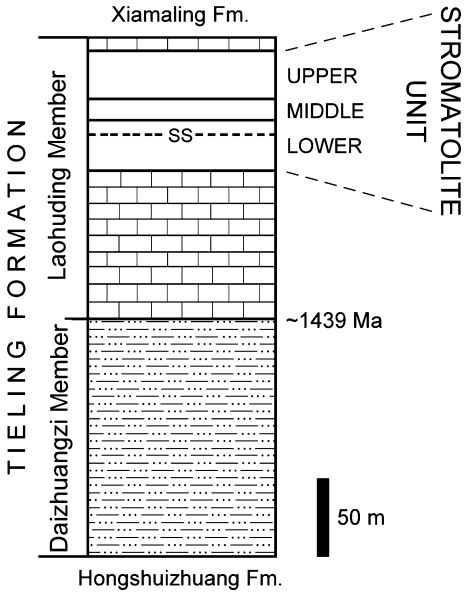

Fig. 2. Stratigraphy of the Tieling Formation in its type area, 5 km north of Jixian city (Chen *et al.*, 1980). The Stromatolite Unit (most of the upper part of the Laohuding Member) is successively dominated by elongate columns (Lower), large domes (Middle) and rounded columns (Upper). The Lower part contains thin horizons of sinuous stromatolites (SS) (Tosti & Riding, 2016). The mid-Tieling Formation is dated *ca* 1439 Ma (Li *et al.*, 2014).

the age of the top of the Tieling. Therefore, the age of the upper (Laohuding) member of the Tieling Formation near Tieling is regarded here as *ca* 1440 to 1400 Ma (late Calymmian). Previously, the Tieling Formation was regarded as 1200 to 1050 Ma (e.g. Chen *et al.*, 1981). The likelihood that it could be substantially older was first indicated by a SHRIMP date of 1368 ± 12 Ma for zircons in a tuff in the overlying Xiamaling Formation near Beijing (Gao *et al.*, 2007).

Localities

Near Tieling village, the Tieling Formation occurs within a NNW–SSE trending syncline (Fig. 1). The Stromatolite Unit has been extensively quarried in the synclinal core between Tieling village and Nanchedaoyucun to the north. Additional smaller quarries occur on the western limb towards Nantaoyuan to the south (Fig. 3). This study describes the branched upright columns of the lower part of the Stromatolite Unit exposed at Tieling Geopark and in the Roadside Section, together with large quarried blocks near the Roadside Section that display bedding plane features. These localities are on the low north–south ridge formed by the western limb of the syncline west of Tieling. The Roadside Section is a quarry south of the road 300 m north-west of the northern end of Tieling village. The 'Tieling Geopark' is a national nature reserve, 750 m south of the Roadside Section and 300 m ENE of Nantaoyuan village. At both localities, the Stromatolite Unit dips east/ESE at about 20 to 30 degrees. From the road north of Nantaoyuan, the Geopark section is accessed by a sinuous pathway that passes eastward (up-section) to the road south of Tieling. From the west, the path crosses the base of the Laohuding Member *ca* 80 m east of the road near Nantaoyuan. Continuing south-east, the path passes small outcrops of laminated carbonate mudstone and flat-pebble conglomerate in the lower part of the Laohuding Member. The base of the Stromatolite Unit, 93 m stratigraphically above the base of the Laohuding Member, is marked by flat-pebble conglomerates colonized by stromatolites. A short distance higher in the succession, the Old Quarry Section is a sinuous north-facing cliff *ca* 50 m long and *ca* 4 m high, representing the uppermost face of a much larger, now infilled, quarry. It includes good end-on exposures of branched elongate columnar stromatolites (Fig. 4) in the Lower Stromatolite Unit. From the Old Quarry Section, the pathway descends steeply to the north-east over a horizontal distance of *ca* 100 m to the base of a small valley (Valley Section) and continues through the Middle and Upper parts of the Stromatolite Unit, and then through the topmost non-stromatolitic 10 m of the uppermost Laohuding Member to the top of the Tieling Formation at its contact with the overlying

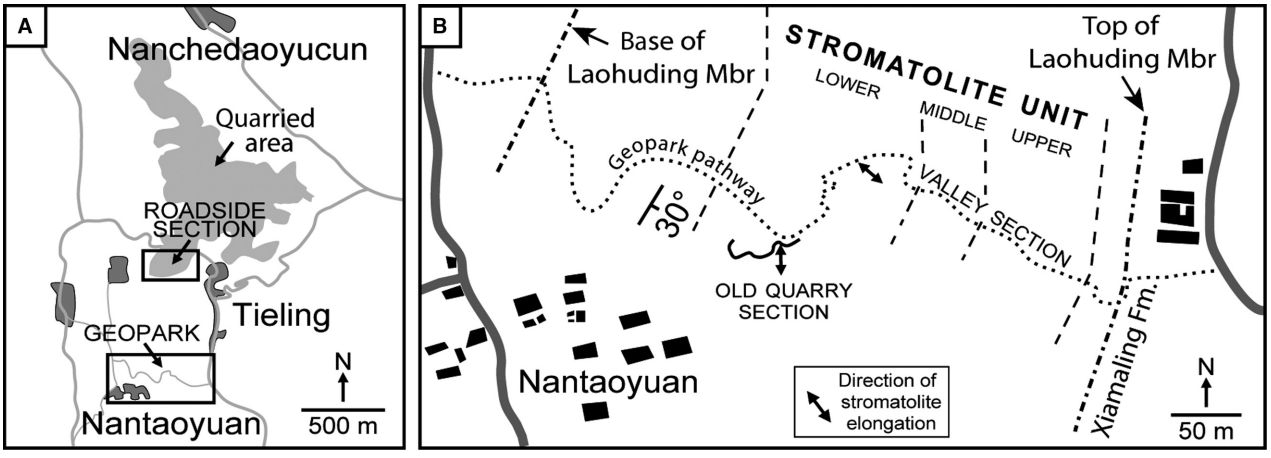

Fig. 3. Tieling localities. (A) Tieling Formation type area. The stromatolite-dominated upper Laohuding Member crops out along a low north–south ridge between Nanchedaoyucun and Nantaoyuan and is extensively quarried north of Tieling. This study examined it in the Roadside Section and at Tieling Geopark. (B) Tieling Geopark showing the three subdivisions of the Stromatolite Unit exposed along the pathway. The remaining thick lower and thin uppermost parts of the Laohuding Member consist mainly of bedded micrite and flat-pebble conglomerate. This study focuses on the Lower Stromatolite Unit which is dominated by elongate columns.

Fig. 4. Part of the Lower Stromatolite Unit, showing thick (1 to 2 m) flat-bedded units uniformly composed of elongate branched columnar stromatolites. Each column is typically *ca* 5 cm wide and flanked by narrow vertical matrix-filled runnels. Columns are erect except for two thin horizons of sinuous columns in the right-hand face. Laohuding Member, Old Quarry Section, Tieling Geopark. Width of view *ca* 14 m. See Fig. 6 for detail.

Xiamaling Formation, *ca* 75 m west of the road south of Tieling village.

Flat-pebble conglomerate and carbonate mudstone

The lower and uppermost parts of the Laohuding Member in the Geopark section (i.e. below and above the Stromatolite Unit) consist of thin-bedded laminated micrite with horizons of flat-pebble conglomerate (also known as 'edgewise conglomerate', Fenton & Fenton, 1931; and 'edgewise mud breccia', Fenton & Fenton, 1937) (Fig. 5). The flat-pebble conglomerate consists of plates about 1 cm thick, some of which are slightly bent suggesting only partial initial lithification (Fig. 5C). These reflect layers of cohesive carbonate mud disrupted by current effects, but without microbial trapping. Stromatolite colonization of flat-pebble conglomerate marks the base of the Stromatolite Unit at the western edge of the Geopark (Fig. 5C), and resembles deposits of similar age in Laurentia (Horodyski, 1976a, fig. 6d).

X-ray diffraction analyses and mineralogy

The stromatolites and their associated matrix are pale yellow to pale grey in outcrop and can be pink in cut slabs. Samples from the Stromatolite Unit were examined using a 'Bruker D2 PHASER' X-ray Diffractometer with LYNXEYE detector (Bruker Corporation, Billerica, MA, USA). Analyses were performed at 30 kV, 10 mA in continuous scan mode from 10 to 90 theta, step 0·02, time 0·1. Ten samples were analysed: six (J50 stromatolite/J50 matrix, J51 stromatolite/J51 matrix; J53 stromatolite; J57 matrix) from the Old Quarry Section (Tieling Geopark) and four (J58 stromatolite/J58 matrix; J62 stromatolite/J62 matrix) from the Roadside Section northwest of Tieling. These values indicate that Tieling stromatolites and matrix as a whole are *ca* 79% calcite and *ca* 19% dolomite (Table 1). The stromatolite (S) samples average 86·6% calcite, 12·0% dolomite, 1·4% clay and other minerals; and the matrix (M) samples average 71·6% calcite, 26·4% dolomite, 2·0% clay and other minerals. Glauconite and chert are present throughout the Tieling Formation (Su *et al.*, 2010). Small amounts of glauconite are commonly present near the margins of the stromatolites. Mei *et al.* (2008) suggested that this glauconite formed as colloidal films at the contact between the stromatolite columns and the intervening unlaminated matrix (which were misidentified as leiolite).

LOWER STROMATOLITE UNIT

This study focuses on outcrops of the Lower Stromatolite Unit dominated by branched elongate columns at Tieling Geopark (Old Quarry Section and western part of the Valley Section) and in the Roadside Section (Fig. 3) including large loose quarried blocks. Established terms are used here to describe stromatolite

morphology (e.g. Glaessner *et al.*, 1969; Raaben, 1969; Cao & Bian, 1985). In the Geopark Section, the Stromatolite Unit is a well-bedded, apparently continuous, 77 m thick succession, divisible into three parts based on stromatolite morphotypes (Fig. 2). From base to top:

Fig. 5. Carbonate mud and flat-pebble conglomerate fabrics in the lower Laohuding Member, north of Nantaoyuan, Tieling Geopark. (A) Laminated carbonate mudstone. Width of view 20 cm. (B) Plate-like clasts of carbonate mudstone in flat-pebble conglomerate showing synsedimentary plastic deformation. (C) Stromatolites colonizing flat-pebble and other carbonate mudstone clasts at the base of the Lower Stromatolite Unit.

1 Lower Stromatolite Unit (Old Quarry Section and western Valley Section): 32 m of narrow, vertically branched, laterally elongate columns that form wall-like ridges.

2 Middle Stromatolite Unit (mid-Valley Section): 13 m of broad domes composed of wide branched columns.

3 Upper Stromatolite Unit (eastern Valley Section): 32 m of narrow, mainly closely spaced and unbranched, but bridged, columns up to *ca* 10 cm wide that include both elongate and rounded forms.

At the eastern end of the Geopark Section, the Stromatolite Unit is overlain by 10 m of laminated micrite and flat-pebble conglomerate in the uppermost Laohuding Formation. These are disconformably overlain by sandstones of the Xiamaling Formation.

The Lower Stromatolite Unit consists of thick (0·5 to 1·5 m) laterally persistent planar beds (Fig. 4), without channel-like gaps or any mound-like or lenticular structures. The sole components are columnar stromatolites and intervening matrix. The columns are upright, except for two thin layers (total *ca* 50 cm) dominated by sinuous, curved and locally toppled columns within the normal succession of erect

Table 1. Estimated weight percent X-ray diffraction mineralogy of ten samples of stromatolite (S) and associated matrix (M) from the Stromatolite Unit (Laohuding Member, Tieling Formation).

Sample	Calcite	Dolomite	Other minerals
J50S	96	3	1
J50M	82	15	3
J51S	75	24	1
J51M	51	48	1
J53S	93	5	2
J57M	90	9	1
J58S	84	15	1
J58M	62	35	3
J62S	85	13	2
J62M	73	25	2
Average	79·1%	19·2%	1·7%

Samples J50S, J50M, J51S, 51M, J53S and J57M are from the Old Quarry Section (Tieling Geopark). Samples J58S, J58M, J62S and J62M are from the Roadside Section north-west of Tieling. Stromatolite (S) samples average 86·6% calcite, 12·0% dolomite, 1·4% clay and other minerals; matrix (M) samples average 71·6% calcite, 26·4% dolomite, 2·0% clay and other minerals. Together, stromatolite and matrix are approximately 79% calcite, 19% dolomite and 2% other minerals.

branched columns in the Old Quarry Section (Fig. 6) (Tosti & Riding, 2015).

Ridge–runnel system

The closely spaced, mutually aligned, upright elongate columnar stromatolites resemble books on a shelf; they are generally separated from one another by vertical matrix-filled spaces, although locally they can be closely juxtaposed (Fig. 6). On the sea floor, the tops of the exposed columns would have been narrow ridges separated by narrow matrix-filled depressions, here termed runnels (Fig. 7). This distinctive 'ridge–runnel' system patterns the bedding plane surfaces (Figs 7 and 8). In the Old Quarry, the ridge–runnels are aligned north–south. Stratigraphically slightly higher, in the western part of the Valley Section, the alignment is north-west/south-east (Figs 3B and 8C) and locally, the runnels almost disappear, leaving adjacent stromatolite ridges laterally juxtaposed. Bedding plane views show (Fig. 8) that the upright wall-like or tile-like stromatolite columns are laterally discontinuous. They typically form sinuously elongate ridges 10 to 40 cm long that locally divide or merge, but can also be rounded to ovoid. Overall column elongation (length/width) values in plan view are generally in the range 2 : 1 to 10 : 1. Despite these variations, both columns and runnels often appear to maintain relatively constant widths (Fig. 8B), and although individual ridges do not continue for more than *ca* 40 cm (Fig. 8A), the associated interconnected runnels are traceable for long distances. The present

Fig. 6. Details of Fig. 4 showing end-on views of elongate stromatolite morphotypes, including branched upright columns (pen and below), sinuous and broken columns (middle) and upright mainly unbranched columns (top). The overall vertical length of the branched column to the right of the pen is 60 cm. This density of stromatolite development is typical of the Stromatolite Unit. Laohuding Member, Lower Stromatolite Unit, Old Quarry Section, Tieling Geopark. Pen is 13·5 cm long.

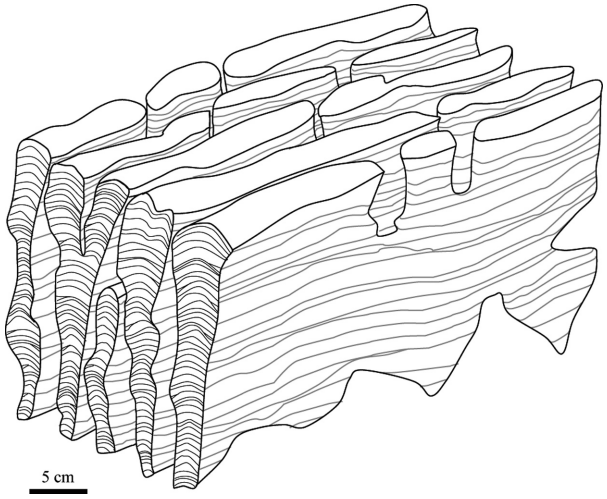

Fig. 7. Interpretation of aligned branched column morphology in the Lower Stromatolite Unit at Tieling. Upright slab-like stromatolites, with inferred irregular margins, branch vertically and are separated by narrow matrix-filled runnels. Column top surfaces exposed on the sea floor accreted vertically, while their margins expanded or contracted with fluctuations in mat matrix relative accretion rate. This phenomenon resulted in upward column expansion or termination, as well as branching. Similar, but horizontal, variations caused columns to end, divide or amalgamate laterally. These changes were reciprocated in the pattern of adjacent runnel development. Depending on the viewpoint, these slab-like columns therefore presented contrasting appearances: end-on – upright branching columns, side-on – extensive subhorizontal sheets, plan view – disjunct elongate ridges and adjacent runnels. Additional angles of section produce further variants. Scale is approximate.

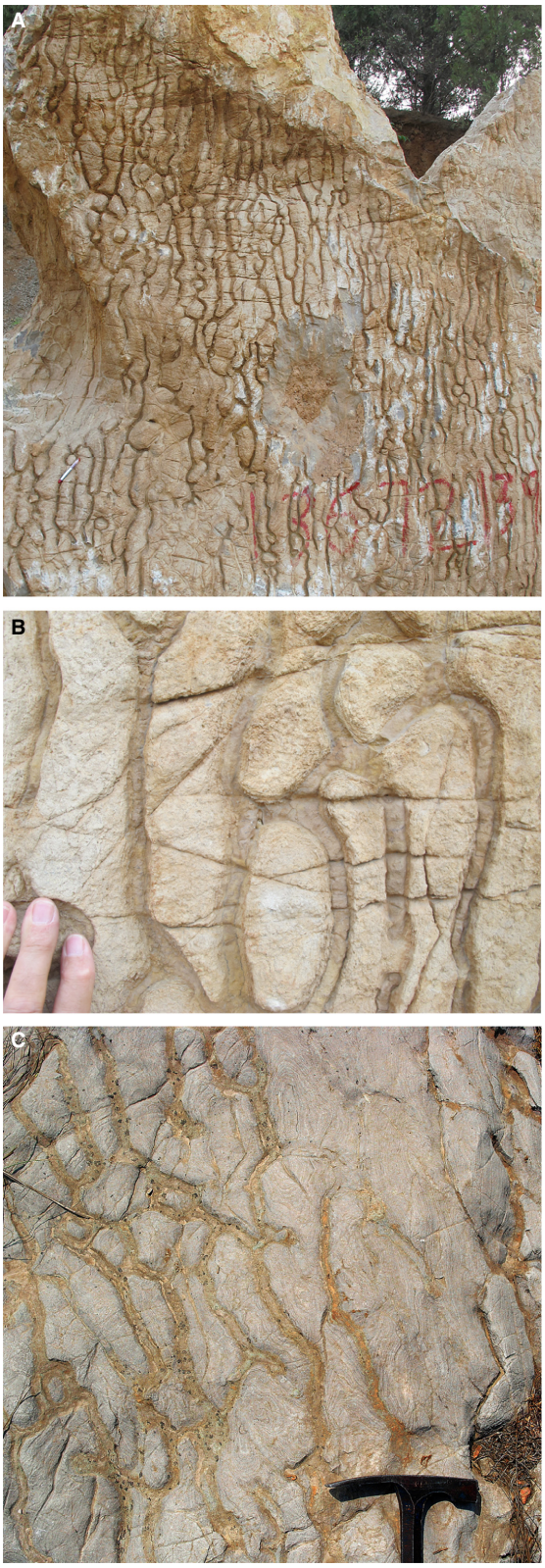

Fig. 8. Ridge–runnel systems in plan view (Laohuding Member, Lower Stromatolite Unit). (A) Aligned discontinuous sinuously elongate stromatolite ridges up to 55 cm (mainly 10 to 40 cm) in length and 2·0 to 7·5 cm (mainly *ca* 3 to 5 cm) wide), separated by narrow continuous runnels. Note the local subcircular columns up to *ca* 5 cm across. Width of view 2·2 m. Loose quarried block north-west of Roadside Section near Tieling. (B) Detail of (A) showing even width and dark fine-grained matrix of the narrow runnels. (C) Eroded ridge–runnel surface revealing stromatolite lamination and showing lateral column separation and amalgamation. Western Valley Section, Tieling Geopark. Hammer head for scale is 16 cm wide.

authors infer that the lower and lateral margins of these upright slabs are somewhat irregular (Fig. 7).

End-on, the upright columns show rapid vertical changes in width that accompany parallel to slightly divergent branching (Figs 6 and 9). Individual columns can extend vertically for 60 cm or more, and are 1 to 9 cm, commonly *ca* 3 to 6 cm, in width. The intervening runnels are up to 8 cm, generally 1 to 3 cm, in width and often maintain relatively even spacing (Figs 8 and 10). Their U-shaped floors accumulated carbonate mud interlayered with carbonate silt–sand intraclasts, some of which are millimetric flakes in a pack of cards structure (Fig. 11). These Tieling intraclasts resemble those between Belt-Purcell columns (Horodyski, 1976a; fig. 7a), and also 'splinters' associated with *Tilemsina* stromatolites in Atar (Bertrand-Sarfati & Moussine-Pouchkine, 1985, figs 9b and c), but are less abundant.

Stromatolite lamination

The columns consist of well-defined laminae, generally <5 mm thick, with sub-layers in the range 1·0 to 1·5 mm. In end-on vertical section, the laminae define low domes with synoptic relief generally less than *ca* 2 cm (Fig. 11). Along the columns, in side view, the lamination is sub-horizontal and undulose (Figs 7 and 12B). Laminar inheritance can be moderately good (Fig. 12); but, erosive cross-cutting, lamina amalgamation and rapid horizontal changes in thickness and width associated with lateral column migration are all common (Fig. 13). Except in very narrow columns, lamina truncation tends to be concentrated nearer the column margins (Fig. 14). Laminae are commonly non-enveloping, columns generally lack walls, and margins are commonly ragged and low angle (Fig. 13C), but steeper partially enveloping

Fig. 9. Upright branched columns ('1' to '6'), separated by interspaces ('a' to 'e'), showing well-defined lamination and changes in width. Interspaces are generally narrower than adjacent columns. Columns 3 to 5 branch from the same column (out of view, below). Column 2 widens upward and then narrows towards the left. Column 3 branches and its right branch terminates upward. Column 4 terminates but then continues. Column 5 narrows and then expands. Many laminae show lateral changes in thickness and discontinuity. Laohuding Member, Lower Stromatolite Unit, Old Quarry Section, Tieling Geopark.

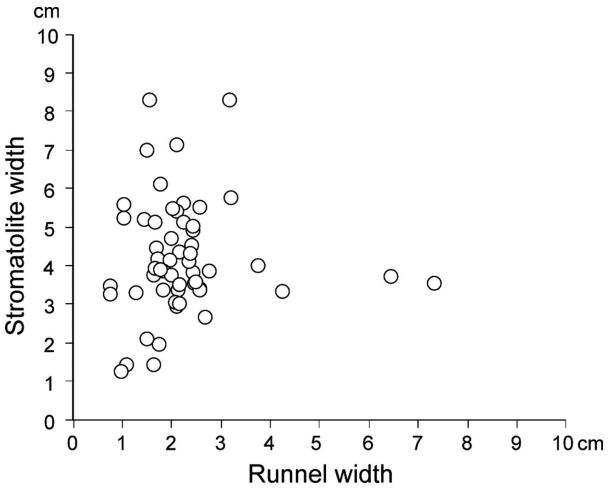

Fig. 10. Stromatolite (i.e. column) width plotted against runnel (matrix) width; data from Laohuding Member, Stromatolite Unit, Old Quarry Section. Column widths range from 1 to 9 cm, mainly 3 to 6 cm. Runnel widths range up to 8 cm, mainly 1 to 3 cm. Rough linear correlation supports the notion of dimensional self-organization in response to factors such as interaction of current generated scour and sedimentation with mat trapping/stabilization.

laminae also occur locally (Fig. 13C). The most common lamina shape is low domical, but angular and flat crests also occur, and can be close together (Fig. 13C). Lamina height is generally low, with a synoptic relief ratio of *ca* 1 : 2 to 1 : 4 (Fig. 15), but conical laminae are occasionally present (Fig. 16) and may have developed in protected interspaces. Although the Tieling succession is generally well-preserved, compactional deformation – in addition to syndepositional breakage – is noticeable in the horizon of curved and sinuous columns, and includes snapped columns and breakage along laminae, especially close to angles of curvature (Tosti & Riding, 2016). Notably, upright columns do not show syndepositional breakage, but small-scale minor structural deformation is present, especially at column margins (Fig. 13B).

Tieling lamination is distinctive; it is well-defined and relatively smooth, but evidently not isopachous. Rapid change in thickness and numerous truncations suggest agglutinating

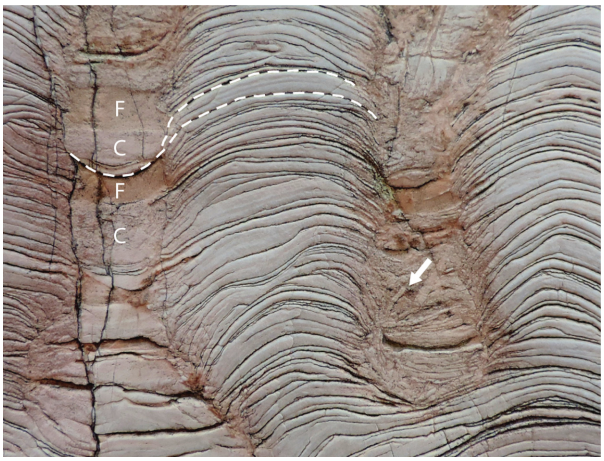

Fig. 11. Branched columns with adjacent matrix-filled runnel interspaces. Well-defined laminae show rapid lateral thickness changes and numerous truncations. Fainter microlamination is also present. Synoptic relief from base of runnel floor to top of adjacent coeval laminae (dashed lines) is *ca* 1·5 to 2·0 cm, depending on which lamina is chosen. The runnels contain coarse 'C' and fine 'F' matrix, as well as small intraclast flakes (arrow). Note that the runnel floor is more U-shaped below coarser matrix, suggesting current scour. Laohuding Member, Lower Stromatolite Unit, Old Quarry Section, Tieling Geopark. Width of view is 11 cm.

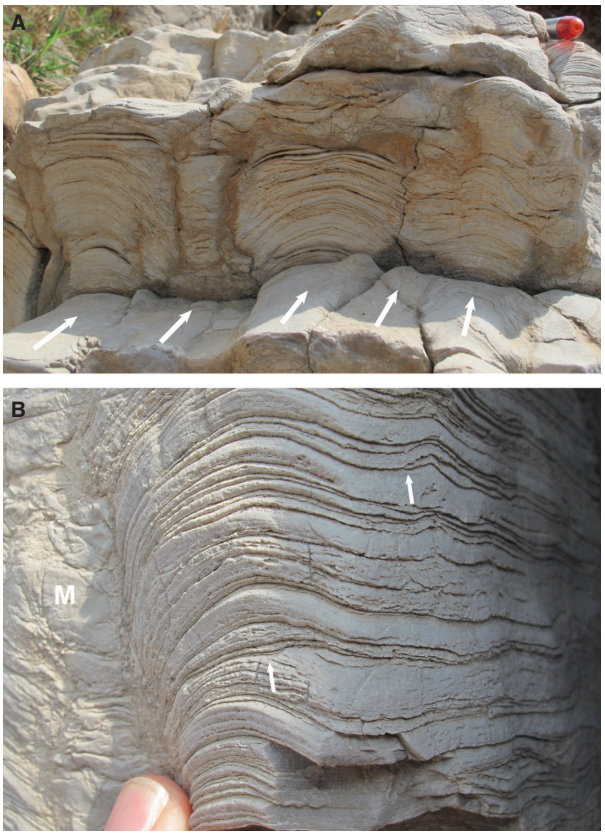

Fig. 12. Elongate columnar stromatolites in vertical view. (A) Aligned elongate upright columns. Arrows indicate elongation trends. Note the close, locally juxtaposed, column spacing with narrow runnel interspaces. Width of view 40 cm. (B) Oblique view showing transverse (left) and longitudinal (right) sections of elongate column; 'M' is intercolumn matrix; stromatolite laminae show erosional truncations (arrows) and are undulose to cuspate in longitudinal section. Laohuding Member, Lower Stromatolite Unit, Old Quarry Section, Tieling Geopark.

accretion in which carbonate mud, transported by relatively strong currents, was trapped and stabilized by cohesive but otherwise only weakly lithified mats. Dupraz *et al.* (2009) suggested that: "trapping and binding of sediment alone will not produce laminated stromatolites". This view, based on present-day coarse-grained agglutinated fabrics in which lamination can be produced by thin precipitated micritic laminae (Reid *et al.*, 2000), is supported by similarly coarse ancient examples (Suárez-González *et al.*, 2014) but it does not apply to fine-agglutinated fabrics at Tieling, which lack signs of precipitated laminae. Instead, Tieling lamination appears to have been produced mainly by pauses in accretion, the most prominent of which are evidently also erosional. Tieling lamination therefore conforms to the definition by Monty (1976) of repetitive lamination: "superposition of laminae of similar nature and configuration, separated by physical discontinuities". It contrasts with the alternating lamination reported from coarse-grained agglutinated stromatolites (Reid *et al.*, 2000; Seong-Joo *et al.*, 2000; Suárez-González *et al.*, 2014).

Microfabric

In thin section, the stromatolite columns, which appear uniformly fine-grained in hand specimen, consist of discontinuous sub-millimetric (commonly 50 to 200 μm) laterally impersistent irregular lenses and layers of micrite, separated and interspersed by similarly thin microspar-dominated layers (see also Mei *et al.*, 2008, figs 3, 4a, b) (Fig. 17). The microspar layers preferentially occur in the stromatolites. This could suggest that they were precipitated *in situ*. However, the microspar shows a very patchy distribution and is closely associated with features, such as lensoid microfabric (Fig. 19A and C), that appear to have been produced by

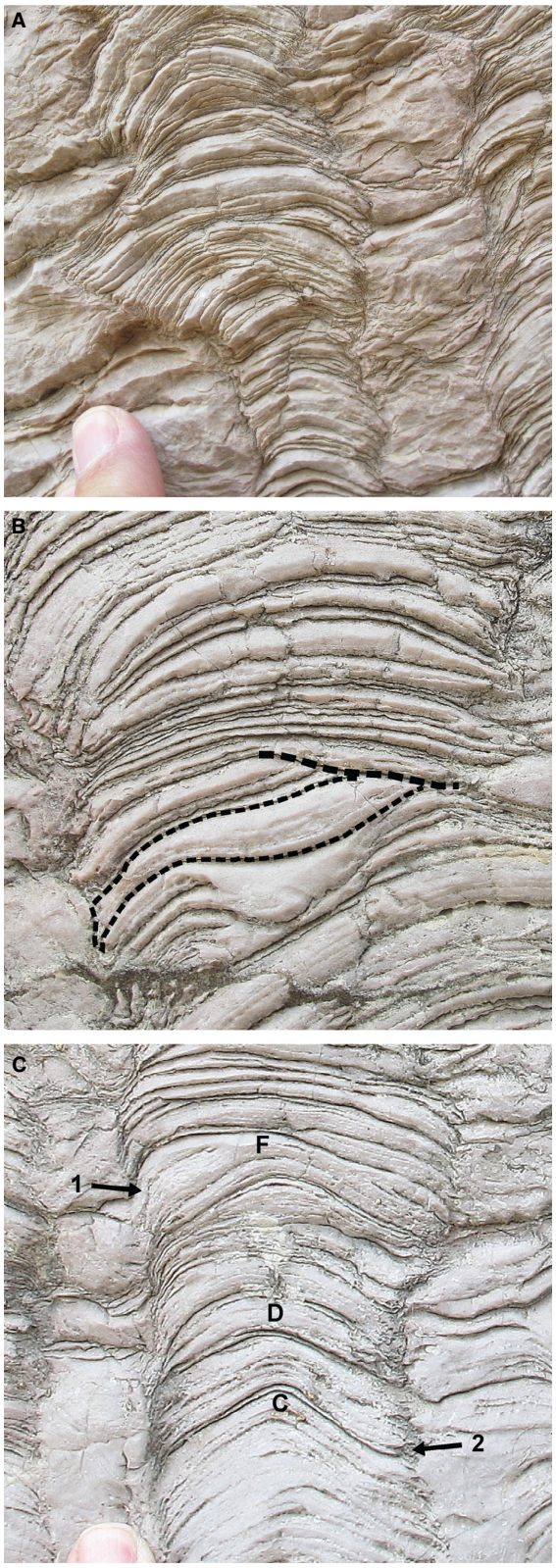

Fig. 13. (A) Stromatolite (centre left), between subvertical matrix-filled runnels. Fluctuation in column width includes lateral lamina migration to left (above finger). In contrast, the margin of the column on the far right shows little change in position. These changes in column margin position reflect fluctuations in mat growth and sedimentation. Note that columns and matrix are both fine-grained. (B) Outlined lamina shows rapid change in thickness, together with erosive truncation. Note the localized deformation of column margin laminae on the left. Width of view 5 cm. (C) Laminae can show good inheritance, but also changes in shape that include low cone 'C', low dome 'D' and flattened 'F'. Several laminae, including 'F', show downturned, partially enveloping, margins (arrow 1), whereas low-relief margins often appear ragged (arrow 2). Laohuding Member, Lower Stromatolite Unit, Old Quarry Section, Tieling Geopark.

deposition of initially unlithified sediment. No fabrics have been observed here that would suggest *in situ* precipitation, such as vertically oriented crystals with terminations, in the microspar that is juxtaposed with matrix at the stromatolite surface (for example, Fig. 18); therefore, this is regarded as selective alteration of an essentially fine-grained precursor. It resembles 'streaky' or 'platy' (Walter, 1972) and 'film' (Bertrand-Sarfati, 1976, fig. 1) microfabric, which Bertrand-Sarfati (1976) considered to be common near the mid–late Riphean transition (*ca* 1·0 Ga). The selective nature of this alteration is seen at column margins where 'streaky' column fabric is juxtaposed against partially dolomitized, but otherwise relatively unaltered, fine-grained matrix in the runnels (Fig. 18). Glauconite is also often localized near column margins (Mei *et al.*, 2008) (Fig. 18D). Column microlayering evidently broadly follows original fabric variations; it includes stromatolitic microcolumns, shows cross-cutting relationships between laminae and preserves small intraclasts that locally include millimetric plates arranged in a pack of cards structure (Fig. 19), together with smaller rounded grains, some of which resemble catagraphs figured by Bertrand-Sarfati (1976, fig. 3b). However, areas of more homogeneous fine-grained microfabric are also present (Fig. 17D), and these have also been seen elsewhere (e.g. Bertrand-Sarfati, 1976, fig. 3a). Lamina contacts are often stylolitic (i.e. 'stylolaminated', Logan & Semeniuk, 1976) (Fig. 17). Fabrics typical of *in situ* mat precipitation (for example, clotted–peloidal, sparry crust, birdseye fenestrae and calcified microbes) are absent. The primary component of Tieling columns therefore appears to have been carbonate mud that was sufficiently coherent to form small flakes and aggregates, but probably did not

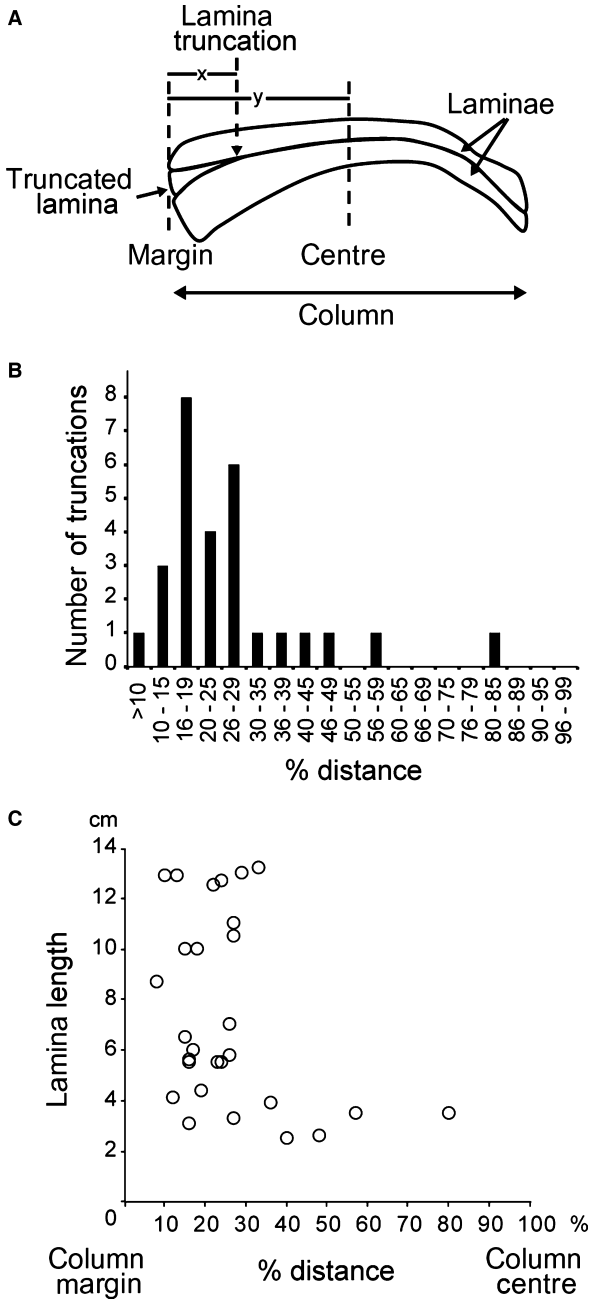

Fig. 14. Lamina truncation. (A) Measurement (based on Fig. 6) of lamina truncation distance from column margin (x) relative to column centre (y). In this example, x/y = 40%. (B) Frequency plot of percent truncation distances (x/y) from column margins to centres measured in the Stromatolite Unit at the Old Quarry Section, Tieling Geopark. Most x/y values are ≤30, i.e. relatively close to the column margin. (C) Plot of (x/y) data from (B), against lamina length (LL). In narrower (lower LL) columns, truncation points approach within 80% of the column centre. In wider columns (higher LL), truncation points are <40% of the distance from the column margin. Thus, overall, truncations occur widely across narrow (LL <5 cm) columns, but nearer the margins of wider (LL >5 cm) columns.

strongly resist erosional scour along the sides and tops of the stromatolites. In addition to neomorphic microspar, cement spar occurs locally between intraclast plates (Fig. 19D). Bertrand-Sarfati (1976) compared film microfabric with Andros tidal flat mats formed by alternation of layers of carbonate mud, with and without *Scytonema* (Monty, 1965), and which are similar to 'type A' mats of Black (1933, pl. 22, fig. 21) (see also Ginsburg & Lowenstam, 1958, pl. 1c). Bertrand-Sarfati (1976) also compared film microfabric with very fine (5 to 10 μm) layers in small coniform geyser-associated stromatolites at Yellowstone National Park described by Walter *et al.* (1976).

Stromatolite names

Gao *et al.* (1934) recognized abundant stromatolites in the Tieling Formation and described *Collenia chihsienensis*. Cao & Liang (1974) identified *Anabaria* and *Baicalia*, based a new genus *Chihsienella* on *Collenia chihsienensis* and created the additional new genera *Pseudotielingella* and *Tielingella* (the authorship of these taxa is Liang & Cao, in Cao & Liang, 1974). In addition to *Baicalia* and *Chihsienella*, the overall Tieling stromatolite association typically contains *Anabaria*, *Tielingella*, *Paraconophyton*, *Scopulimorpha* and *Pseudochihsienella*, and this has been listed as one of China's five distinctive mid–late Proterozoic stromatolite assemblages (Chen *et al.*, 1981; Cao & Yuan, 2003). Riding (1991; 2000, fig. 8) described and figured fine-grained well-laminated stromatolites from Tieling Geopark. Cao & Yuan (2003) recognized *Conicodomenia* and *Conophyton*, and noted 'large biostromes of great thickness' formed by abundant and diverse columnar branching stromatolites. Zhou *et al.* (2009, fig. 1) described the Stromatolite Unit as a series of species of *Scopulimorpha*, *Baicalia*, *Anabaria*, *Pseudotielingella*, *Tielingella*, *Chihsienella*, *Conophyton* and *Conicodomenia*. The term 'columnar' usually implies a more or less rounded to ovoid cross-section, and this would typically describe *Anabaria* and *Baicalia* (Raaben, 1969). Information signs in Tieling Geopark in 2013 described stromatolites in the Old Quarry and western Valley Sections as *Anabaria* and *Baicalia*, even though they are ridged in longitudinal section. In the eastern Valley Section, signs identified branched ridge-like elongate columns as *Scopulimorpha*, and closely spaced, unbranched, bridged columns, up to *ca* 10 cm wide as *Chihsienella* and *Tielingella*.

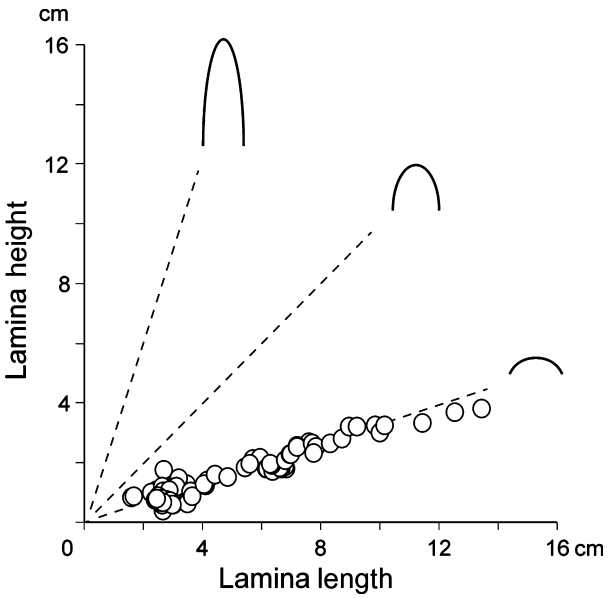

Fig. 15. Lamina height plotted against lamina length for columns in the Lower Stromatolite Unit at the Old Quarry Section. Lengths are mostly 2 to 10 cm and heights mostly <3 cm; i.e. narrow columns with relatively low relief. Good correlation suggests a general response to controlling factors such as interaction of current-influenced sedimentation and mat trapping. It is inferred here that low-relief columns were prone to branch as column accretion responded to sediment supply.

Fig. 16. Coniform column (right) adjacent to low-relief columns. Although these columns are probably elongate they suggest that fine agglutination can produce conical crests. Note the vertical gradation from coniform to curvilinear lamina appearance. Laohuding Member, Stromatolite Unit, Roadside Section north-west of Tieling village.

The aim here is to interpret these deposits, rather than to rationalize or refine their taxonomic nomenclature; but the present authors note that *Chihsienella* (*Collenia chihsienensis*) is a bridged columnar, rather than branched, form (see Gao *et al.*, 1934, fig. 5). Furthermore, the vertically branched stromatolites that dominate the western Valley and Old Quarry Sections are distinctly elongate, creating the ridge–runnel systems described here. These stromatolites are therefore unlike typical *Anabaria* and *Baicalia*, and can be compared much more closely with species attributed to *Platella* Korolyuk; in particular, *P. talwarensis* Raha (1980) (see Raaben *et al.*, 2001). *Platella* was first described from the Debengde Formation in the Olenek Uplift, northern Siberia (Korolyuk, 1963), and Serebryakov (1976) illustrated sinuous *Platella* from the Debengde. Debengde dates include 1241 Ma (Veselovskiy *et al.*, 2009) and 1272 to 1211 Ma (Gorokhov *et al.*, 2006).

INTERPRETATION

Depositional environment

Studies focused on glauconite in the sequence have interpreted the stromatolites as high-energy shallow subtidal marine deposits (Mei *et al.*, 2008; Zhou *et al.*, 2009). Mei *et al.* (2008, fig. 1) regarded each of the two Tieling members (Daizhuangzi and Laohuding) as third-order sequences capped by palaeokarst, with the Daizhuangzi highstand facies being intertidal manganiferous dolomite and shale, and the Laohuding highstand facies being high-energy shallow subtidal stromatolite-rich dolomitic limestone (i.e. the Stromatolite Unit). The well-defined persistent parallel planar beds (Fig. 4) and aligned ridge–runnel systems (Figs 7 and 8), that characterize the Lower Stromatolite Unit, suggest current dominated – possibly tidal – conditions. Apart from sub-circular and polygon-shaped columns in the Upper Stromatolite Unit, no signs of desiccation or subaerial exposure can be seen. The planar beds of the Lower Stromatolite Unit contrast with more mounded biostromal deposits formed by columnar stromatolites (e.g. Walter, 1972; Young & Long, 1976). Lower Stromatolite Unit elongate columns resemble Palaeoproterozoic examples at Pethei which Hoffman (1989, fig. 8a), with the good control on facies trends provided by extensive three-dimensional exposure, was able to

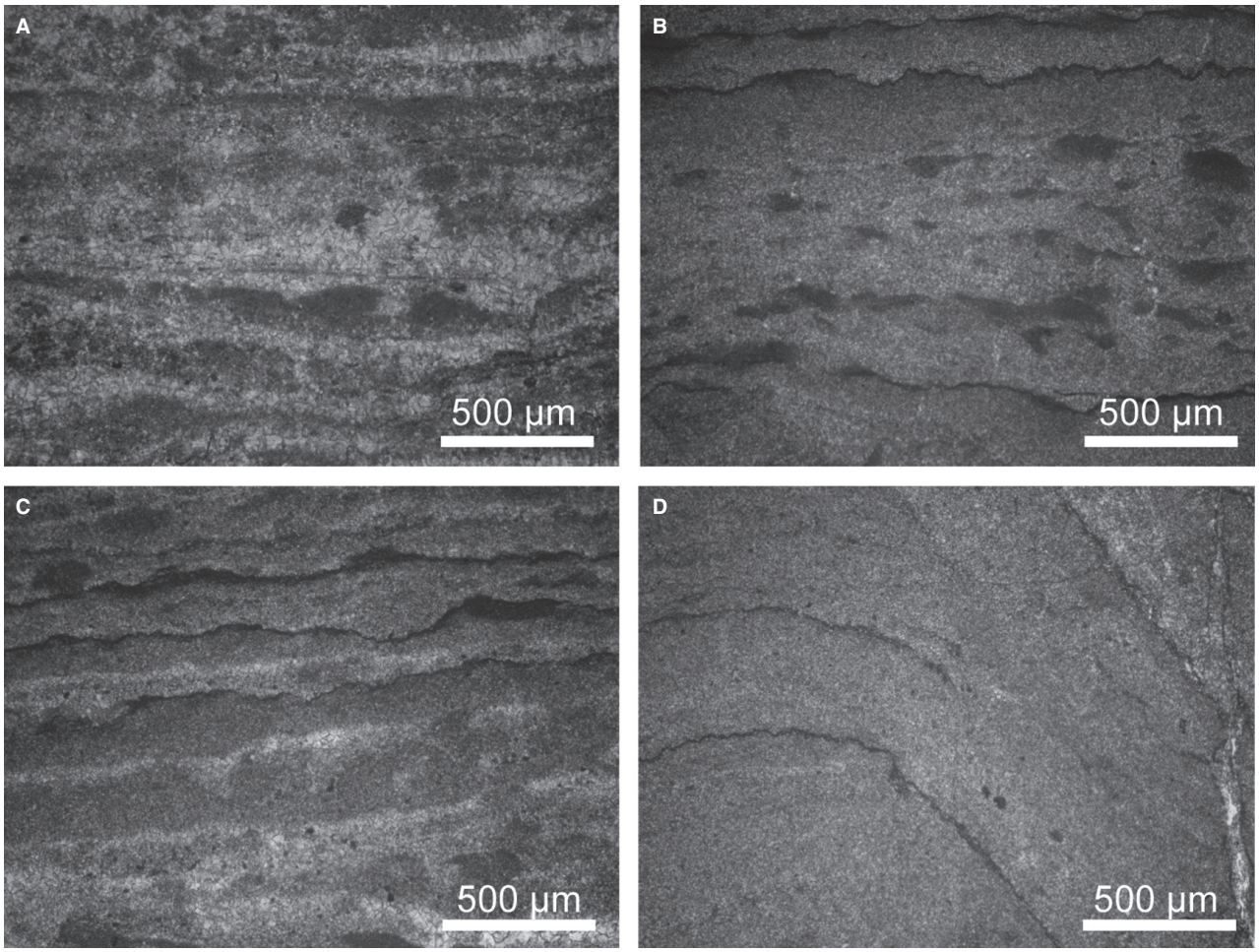

Fig. 17. Laminated, including 'streaky', microfabric. (A) More and less persistent thin layers of micrite and silt-size aggregates (for example, near the top), with thicker microspar bands. (B) Small dark fine-grained lenses in slightly coarser lighter groundmass, with occasional laterally persistent darker stylolite-bounded layers. (C) Similar to (B) but with more persistent layers emphasized by thin microspar horizons. (D) Homogeneous delicately layered fine fabric with stylolitic laminae. Photomicrographs; Laohuding Member, Lower Stromatolite Unit, Old Quarry Section, Tieling Geopark.

interpret as back-reef deposits. The Lower Stromatolite Unit at Tieling can be interpreted broadly as a shallow-marine current-swept deposit, deepening-up to the larger domical columns of the Middle Stromatolite Unit, and shallowing again to less current-influenced deposits dominated by rounded (non-elongate) bridged columns in the Upper Stromatolite Unit.

Reworked allochthonous carbonate mud

The Lower Stromatolite Unit (stromatolites, matrix and intraclasts), together with its immediately underlying and overlying flat-pebble conglomerate deposits, was all originally essentially carbonate mud. Scoured runnel margins, truncated laminae, small flakes, locally deformed columns and flat-pebble clasts all suggest sediment that was sufficiently cohesive to form flakes and plates, rather than early lithified. Persistent current effects are indicated by features on several scales. Rapid lateral changes in lamina thickness and amalgamation indicate repeated erosional reworking of the accreting stromatolite surfaces. The cross-cutting truncations (referred to elsewhere as micro-unconformities by Preiss, 1972, fig. 1) suggest scour and drape erosion, similar to reactivation surfaces, formed by subaqueous erosion as flow direction alters, as in tidal bedforms (de Klein, 1970).

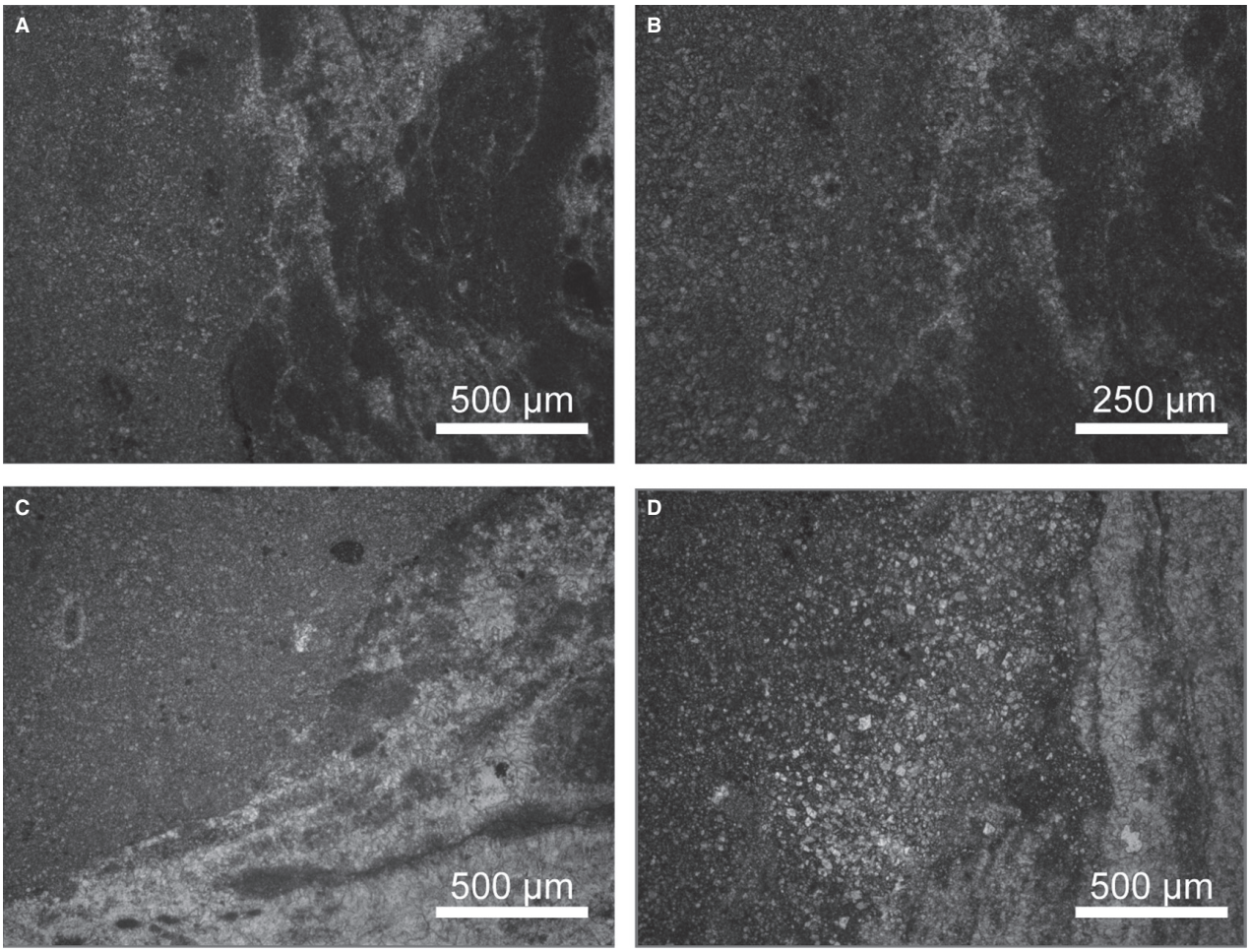

Fig. 18. Contacts between matrix with occasional very fine sand-size grains (left) and stromatolite columns with 'streaky' fabric (right). (A) Relatively well-preserved micritic fabrics. (B) Detail of (A). (C) Micritic matrix contrasting with mainly altered, microsparitic, column. (D) Similar to (C), but with numerous small dolomite crystals (light) and occasional glauconite grains in the matrix. Photomicrographs; Laohuding Member, Lower Stromatolite Unit, Old Quarry Section, Tieling Geopark.

Similarly, even smaller micro-unconformities occur in present-day hypersaline Storr's Lake stromatolites (Paull *et al.*, 1992).

Grain trapping

Tieling low-relief unwalled columns with mainly non-enveloping laminae, show rapid lateral change in margin position and are frequently branched. These features are consistent with low relative accretion rate and mats that accreted mainly by trapping fine-grained particles rather than by *in situ* precipitation (Riding, 1993); they also indicate frequent episodic reworking by currents. Whereas cross-bedding has a lateral growth vector, Tieling laminae dominantly show upward growth that was sufficient to maintain low column relief, but generally did not create synoptic relief of more than a few centimetres. Their scour and drape features resemble subaerial 'adhesion lamination', where grains accrete on moist windward surfaces (Hunter, 1969, 1973; Kocurek & Fielder, 1982). However, Tieling laminae evidently accreted subaqueously and their grain 'adhesion' is interpreted here to have been by microbial mats. Partially eroded laminae reflect preferential synsedimentary scour of column dome margins but, on balance, the mats resisted erosion. In contrast, unstable sediment in the runnels was moved by currents, as shown by coarser layers and pack of cards structures (Figs 11 and 19D). The rare horizons of curved and locally displaced columns suggest that intercolumn

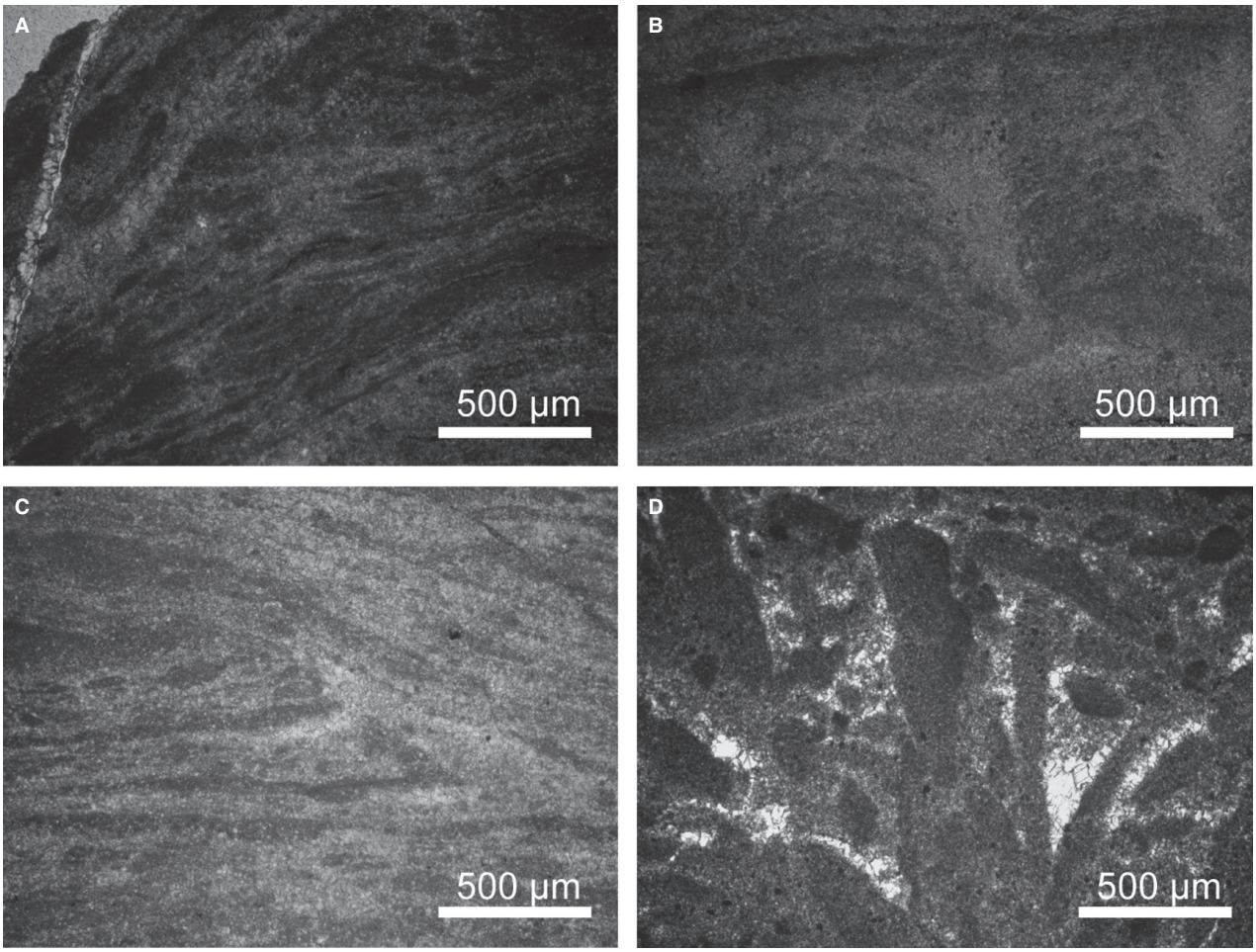

Fig. 19. (A) 'Streaky' column fabric showing erosional truncation surface (upper left). (B) Millimetric microcolumnar fabric within stromatolite column. (C) Similar to (A), but with more microspar. (D) Detail of runnel matrix showing millimetric intraclast flakes in a pack of cards structure. Photomicrographs; Laohuding Member, Lower Stromatolite Unit, Old Quarry Section, Tieling Geopark.

runnels were occasionally sufficiently deeply scoured (possibly by storm events) to cause local column collapse (Tosti & Riding, 2016). The present authors infer that microbial mats were crucial in trapping and stabilizing carbonate mud that otherwise would have been removed by currents.

Vertical branching and lateral ridge–runnel patterns

Vertical fluctuations in column width reflect the ability of mat growth to keep up with sediment supply: oversupply led to branching, lateral separation and local termination of columns; undersupply promoted column expansion, juxtaposition and locally elsewhere in the succession, amalgamation and bridging. Most runnels are narrower than the columns they separate (Fig. 10) and the sea floor was therefore dominated by elongate stromatolitic mats (Fig. 7). At Shark Bay, Logan (1961) observed that water movement "in depressions in the intertidal surface inhibits active mat growth". Similarly, it is inferred here that the runnels at Tieling indicate the inability of the mats to colonize the entire substrate. Thus, mats trapped and stabilized carbonate mud, and high sediment load promoted rapid accretion. Where mat growth only just kept up with sediment supply, the columns became separated by runnels, but where mat growth kept up with or exceeded sediment supply, the columns became juxtaposed, closing the runnels. However, the regularity of the ridge–runnel systems (Figs 8 and 10) reflect an additional and pervasive overriding control on the pattern of columnar mat growth and intervening sediment accumulation,

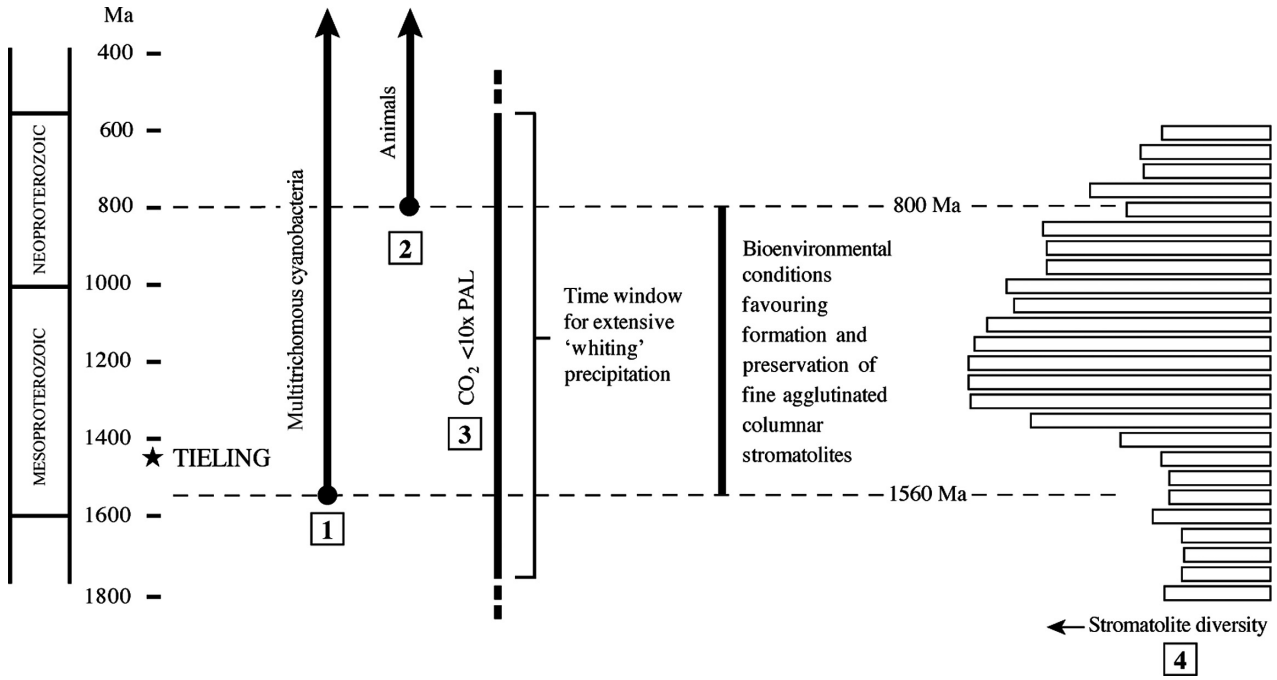

Fig. 20. Bioenvironmental factors favouring formation and preservation of fine-agglutinated columnar stromatolites *ca* 1560 to 800 Ma, based on a copious supply of whiting mud promoted by <10 x PAL CO_2, presence of multi-trichomous mats and absence of animals. At *ca* 1420 Ma, Tieling could be a relatively early example of branched columns created by mat-sediment interactions that contributed to morphotypic diversity in Mesoproterozoic–Neoproterozoic columnar stromatolites. 1. Seong-Joo & Golubic (1998); 2. Erwin *et al.* (2011); 3. Sheldon (2013, fig. 3); 4. Awramik & Sprinkle (1999, fig. 2).

which is inferred to have been persistent currents and/or waves. Whether Tieling ridge–runnels were aligned parallel or normal to prevailing currents remains unclear, since support for either interpretation can be found in present-day and ancient examples (see *Discussion, Stromatolite alignment*).

DISCUSSION

Secular setting

Overviews of shallow-marine Archaean–Proterozoic Ca–Mg carbonate sediments suggest long-term reduction in sea floor crust precipitation (for example, crystal fans, herringbone calcite and microdigitate stromatolites) coupled with increase in fine-grained (micritic) carbonate (Knoll & Swett, 1990; Kah & Grotzinger, 1992; Grotzinger & Kasting, 1993; Grotzinger, 1994; Kah & Knoll, 1996; Altermann, 2008). This trend is thought to reflect decline in seawater carbonate saturation (Grotzinger, 1989a; Grotzinger & Kasting, 1993), which also reduced stromatolite abundance (Grotzinger, 1990). Grotzinger & Knoll (1999) proposed that: "stromatolites were originally formed largely through *in situ* precipitation of laminae during Archaean and older Proterozoic times, but that younger Proterozoic stromatolites grew largely through the accretion of carbonate sediments, most likely through the physical process of microbial trapping and binding. This trend most likely reflects long-term evolution of the earth's environment rather than microbial communities". Tieling stromatolites occur somewhere near the middle of this long-term transition, and it is clear that their formation and preservation required the co-occurrence of several specific factors. These include a copious supply of carbonate mud, microbial mat builders well-adapted to cope with this abundant sediment, and the absence of significant early lithification and also of bioturbation (Tosti & Riding, 2016) (Fig. 20). These factors are considered in turn below.

Carbonate mud source

In present-day carbonates, principal biogenic sources of abundant carbonate mud include water column whiting precipitates and skeletal

disaggregation of green algae such as the bryopsidalean *Penicillus*. Much of the fine-grained carbonate produced internally by fish (Perry *et al.*, 2011) may dissolve in present-day near surface ocean water (Woosley *et al.*, 2012), but was not in any case a Precambrian source of calcium carbonate. It has been suggested that prasinophycean green algae originated by 1200 Ma, probably by 1500 Ma and possibly by 1730 Ma (Teyssèdre, 2006). However, bryopsidaleans are currently estimated to have originated in the Late Neoproterozoic or Early Cambrian (Verbruggen *et al.*, 2009), and the oldest currently known fossil representative of the related group Cladophorales is *ca* 750 to 800 Ma (Butterfield *et al.*, 1994; Knoll, 2014). Thus, although calcified green algae cannot be excluded as a mud source, current estimates suggest that large calcified siphoneous chlorophytes are unlikely to have been extant in the Mesoproterozoic.

In the absence of skeletal carbonate, the ubiquitous mud could have been formed by water column 'whiting' precipitation, stimulated by cyanobacterial photosynthesis. Knoll & Swett (1990) suggested that: "Late Riphean decreases in pCO_2 altered $CaCO_3$ saturation state in the oceans, tipping the balance towards carbonate removal by whitings rather than via precipitation within benthic microbial communities". A water column 'whiting' origin for Proterozoic carbonate mud has often been suggested (Maslov, 1961; Awramik & Riding, 1988; Grotzinger, 1989a, 1990; Herrington & Fairchild, 1989; Knoll & Swett, 1990; Walter *et al.*, 1992; Grotzinger & Kasting, 1993). Under relatively low CO_2 conditions (for example, less than *ca* 10 PAL), picoplanktic cyanobacteria can induce CO_2-concentrating mechanisms (CCM), and Riding (2006) suggested that Mesoproterozoic increase in carbonate mud could reflect decline in atmospheric CO_2 below 10 x PAL CO_2. Sheldon (2013) estimated that CO_2 levels were below 10 x PAL between *ca* 1750 Ma and *ca* 600 Ma. So long as the seawater carbonate saturation state remained sufficiently elevated, this may have sustained intense 'whiting' events that produced copious quantities of mud grade $CaCO_3$ that accumulated on the sea floor. Well-dated Tieling stromatolites, which indicate that well-developed carbonate mud-dominated stromatolite facies were forming *ca* 1440 to 1400 Ma ago, fit this trend and may help to calibrate it (Fig. 20). Present-day whitings are particularly linked to picophytoplankton such as *Synechococcus* (Thompson & Ferris, 1990). However, genomic studies suggest appearance of *Synechococcus* (and also *Prochlorococcus*, SynPro clade) *ca* 0·6 to 1·0 Ga (Blank & Sánchez-Baracaldo, 2010; Blank, 2013; Sánchez-Baracaldo *et al.*, 2014). Thus, if Tieling carbonate mud reflects cyanobacterial bloom-triggered whitings, it could imply that forms such as *Synechococcus* may have been extant at least *ca* 1·4 Ga, in which case estimates based on assumptions inherent in phylogenetic tree calculations should be revised downward.

Microbial mats to trap sediment

Grotzinger & Knoll (1999) noted that sedimentation is essential to accretion, that high sedimentation rates can favour filamentous over coccoid cyanobacteria, and that critically high sedimentation rates can bury mats. Similar conditions can broadly be inferred at Tieling. Gliding motility in filamentous cyanobacteria (Halfen & Castenholz, 1971) has been linked to light optimization/avoidance strategies (Castenholz & Garcia-Pichel, 2012; Moon *et al.*, 2012), as well as to aerotaxy (Whale & Walsby, 1984). Motility also confers the ability to overcome burial (Pentecost, 1984; Whale & Walsby, 1984; Browne *et al.*, 2000). Survival in dark sulphidic burial conditions can be assisted by the ability to switch from oxygenic to anoxygenic photosynthesis, with H_2S as the electron donor, as in the common mat-forming cyanobacterium *Microcoleus chthonoplastes* (Jørgensen *et al.*, 1986), and these cyanobacteria appear to survive dark conditions within mats for up to 10 years (Jørgensen *et al.*, 1988). Under experimental burial conditions, *Microcoleus* filaments can resurface through mud from depths of 5·5 mm in 18 h (Whale & Walsby, 1984), and entire mats buried by 2·5 mm of silt show 'almost complete recovery' within 3 h (Pentecost, 1984). Recovery in part appears to be texture dependent; mats covered by 3 mm of medium-grained sand failed to recover after 6 h (Pentecost, 1984). Repeated burial and recovery has been suggested to impart lamination (Gerdes *et al.*, 2000). Motility within sediment also occurs in benthic diatoms (Round, 1971; Admiraal *et al.*, 1982). Evidently, the ability of microbes to not only trap sediment, but also to survive and recover after burial, is central to the formation of agglutinated stromatolites (Stal, 1995; Seong-Joo *et al.*, 2000; Kromkamp *et al.*, 2007). Silicified fossils of multitrichomous cyanobacteria resembling

Schizothrix and *Microcoleus* have been reported from the lower part of the Gaoyuzhuang Formation north-west of Beijing (Seong-Joo & Golubic, 1998), now dated *ca* 1560 Ma (Li *et al.*, 2013; table 2). Cyanobacteria resembling *Microcoleus* were therefore extant when Tieling stromatolites were forming (Fig. 20).

This study interprets Tieling stromatolites as products of a trapping and binding mat community that stabilized abundant carbonate mud under illuminated, current-swept (probably tide-influenced and storm-influenced), shallow subtidal conditions. Uncalcified cyanobacteria are key components of present-day Andros mats that create laminated domes (Black, 1933), similar to those at Tieling. Silicified (for example, *Siphonophycus*) and calcified (for example, *Girvanella*) filamentous cyanobacteria are locally present in mid–late Proterozoic shallow-marine carbonates (Knoll *et al.*, 1989, 2013; Sergeev, 1994; Kah & Riding, 2007). Black (1933) emphasized that fine-grained agglutinated mats like those at Twelve O' Clock Cay are unlithified, 'without any perceptible addition of secondary crystals', whereas in supratidal areas, *Scytonema* forms 'an entirely different structure' of partly calcified heads with radiating filaments. No evidence of calcified filaments or other signs of microbial precipitation has been observed in Tieling stromatolites. Synsedimentary consolidation was sufficient to create small intraclasts, withstand ambient currents and generally maintain laminar height/width ratios of 1 : 3 (Fig. 15), but did not prevent erosional scour that truncated laminae (Fig. 13B). Coniform laminae with height/width ratios >2 : 1 have been observed occasionally (Fig. 16). Although steeper than most Tieling column margins, these laminae with inclinations of 40 to 75 degrees remain consistent with an origin by grain trapping by filamentous cyanobacteria, based on stabilization studies of fine grains on cyanobacterial mat surfaces at slopes up to 75 degrees (Frantz *et al.*, 2015).

Depressed early lithification

Lack of calcified cyanobacterial filaments in Tieling stromatolites could reflect CO_2 levels that were low enough to promote whiting precipitation, but not to induce sheath calcification (see Riding, 2006). A possible feedback is that intense whiting events, stimulated by phytoplankton blooms, lowered seawater carbonate saturation, further reducing synsedimentary lithification. These conditions may have increased whiting mud at the expense of sheath calcification, thereby enhancing the supply of mud and also the ability of mats to trap it.

Lack of bioturbation

Andros mats

Extensive surfaces of fine-grained carbonate sediment on present-day tidal flats and freshwater marshes at Andros Island are colonized by cyanobacterial mats (Shinn *et al.*, 1969; Monty, 1972; Monty & Hardie, 1976; Hardie, 1977; Maloof & Grotzinger, 2012; Rankey & Berkeley, 2012). Black (1933) compared these deposits with Precambrian and Palaeozoic stromatolites and recognized four types of laminated surface mat. Of these, Type B most resembles Tieling stromatolites and forms smooth rounded convex domes, up to 5 cm high and 12 cm across, in waters of normal marine salinity on tidal mud flats at Twelve O' Clock Cay and wide opening. All four types consist of mud and bioclastic sand 'mechanically entrapped' by cyanobacteria. The description by Black (1933) of trapping and binding was seminal: "The colonization of newly deposited sediment by filamentous algae first of all binds together the sediment, preventing its being easily washed away again, and then produces a felt of algal filaments, which is sometimes quite thick and dense. In nearly all the species involved, the filament is enclosed in a mucilaginous sheath, to which mineral particles very readily adhere. Thus any fresh sediment brought into the region is at once trapped amongst the filaments". Similar mats were subsequently described from south Florida (Ginsburg *et al.*, 1954; Ginsburg & Lowenstam, 1958).

However, the susceptibility of such poorly lithified agglutinated stromatolites to bioturbation greatly limited their preservation during the Phanerozoic. Black (1933) emphasized that Andros mats are generally soft and subsequent studies showed that during early burial, much of their laminated structure is rapidly destroyed by bioturbation (Shinn *et al.*, 1969, fig. 11). Garrett (1970) suggested that weakly lithified stromatolites would only have been well-preserved in subtidal environments prior to the appearance of animals, and pointed out that whereas stromatolites dominated carbonate platforms in the Proterozoic, they are far less extensive at the present day, and that to envisage modern equivalents of such deposits, "we would have to imagine the entire Bahama Banks covered with stromatolites".

Comparison

Tieling fine-grained stromatolites are comparable with several key features of present-day Andros marginal marine mats: (i) copious supply of fine-grained carbonate; (ii) trapping and binding by a microbial community that includes filamentous cyanobacteria; and (iii) only weak initial lithification. However, supratidal mats at Andros commonly incorporate numerous small skeletal bioclasts (Black, 1933; Monty & Hardie, 1976), and the subtidal and intertidal muds are typically faecally pelleted into silt and sand (Shinn *et al.*, 1969). Tieling stromatolites lack sand-size bioclasts and show no signs of faecal pellets. Apart from small intraclasts, also composed of carbonate mud, their primary texture appears to have been wholly fine-grained. Bioturbation adds an even more important difference. Andros mats are only well-laminated close to the sediment surface. In the subsurface, they are generally destroyed by synsedimentary bioturbation (Black, 1933; Shinn *et al.*, 1969; Garrett, 1970). As a result, laminae are rarely preserved except on beach ridges (Shinn *et al.*, 1969). This intense reworking is due to diverse animals, including polychaetes and gastropods. Thus, whereas Andros mats resemble Tieling stromatolites in being relatively fine-grained and lacking early lithification, good lamination is restricted to intertidal forms, and the subtidal deposits are strongly bioturbated. In contrast, Tieling columns preserve fine details of branching and lamination over wide areas and through many metres of vertical thickness. They therefore support the contention of Garrett (1970) that well-laminated stromatolites, formed by processes such as those observed at Andros, were much more likely to be preserved prior to the appearance of burrowing and grazing organisms. Current estimates suggest that eukaryote appearance *ca* 1·6 to 1·4 Ga (Knoll, 2014) was followed by amoebozoan, bikont and opisthokont radiations *ca* 1·0 Ga (Porter & Knoll, 2000; Berney & Pawlowski, 2006), and by animals *ca* 800 Ma (Erwin *et al.*, 2011; Sperling *et al.*, 2013). If so, then the age (*ca* 1·42 Ga) as well as the preservation of Tieling stromatolites are both consistent with the absence of macrofauna and meiofauna (see also Awramik, 1971; Bernhard *et al.*, 2013).

Stromatolite alignment

Ancient examples

Stromatolite alignment has been reported to be normal to shorelines and platform margins (Goldring, 1938; Truswell & Eriksson, 1973; Ricketts, 1983) and has commonly been attributed to the effects of currents (Rezak, 1957; Young, 1974; Young & Long, 1976; Horodyski, 1983, 1989; Pelechaty & Grotzinger, 1989; Bertrand-Sarfati & Awramik, 1992). Tice *et al.* (2011) expected that stromatolites should tend to be elongated along the flow azimuth in moderate to high-energy tidal environments. This view has been supported by comparisons with associated ripple marks and cross-bedding whose current directions parallel stromatolite elongation (Hoffman, 1967, fig. 1; Trompette, 1969; Haslett, 1976, fig. 4; Young & Long, 1976; Ruppel & Kerans, 1987, fig. 13; Cozzi *et al.*, 2004; Hoffman & Halverson, 2011), and for stromatolites elongate normal to shelf margins (Hoffman, 1976a, 1989; Sami & James, 1993). However, because marked changes in stromatolite alignment can occur over thicknesses of *ca* 10 m at Tieling (Fig. 3B), and even over thicknesses <1 m (Serebryakov & Semikhatov, 1974, fig. 4) [in *ca* 1·5 Ga, Sergeev (2009) *Kussiella*], it is debatable whether current direction indications can confidently be extrapolated between even adjacent beds.

Present-day examples

Alignment, normal to low-water mark and parallel to water movement, was noted in elongate stromatolites at the Great Salt Lake (Eardley, 1938; Carozzi, 1962) and Shark Bay (Logan, 1961), and Gebelein (1969) attributed dome elongation to preferential accretion parallel to current direction at Bermuda; but closer examination at Shark Bay revealed complications. For example, some stromatolites are aligned at an angle of *ca* 30 degrees to the shoreline, but parallel to the prevailing wind direction (Playford & Cockbain, 1976). In addition, Hoffman (1976b, figs 6 and 7) noted that intertidal columns are circular in plan view near headlands and elongate perpendicular to the shoreline in adjacent bays (bights), and observed that although individual columns in the bays are elongate parallel to wave and tidal scour, they also tend to occur in 'rows or bands parallel to the shoreline'. At Lee Stocking, subtidal columns 'lean' in the direction of major tidal flow but align normal to this direction, parallel with the crests of submarine sand dunes (Dill *et al.*, 1986). At Shark Bay, Mariotti *et al.* (2014, fig. 5) attributed stromatolite alignment that is parallel to the shore (and to ripple marks), and normal to wave direction, to preferential colonization by mats of sand bar runnels where sediment transport is low,

whereas sand bar ridges experience increased transport.

Ridge–runnel organization

Tieling ridge–runnel stromatolite systems are interpreted here as interaction between: (i) current direction and velocity that transported ubiquitous carbonate mud and could scour the substrate; and (ii) the stabilizing effects of prolific microbial mats. Feedback mechanisms between fluid flow and sediment transport strongly influence shallow water patterns in both siliciclastic and carbonate sediments (e.g. Dyer & Huntley, 1999; Rankey *et al.*, 2006; Coco & Murray, 2007; Holland & Elmore, 2008; Syvitski *et al.*, 2010; Harris *et al.*, 2011), and these can incorporate the influence of vegetation (Kirwan & Murray, 2007; Vandenbruwaene *et al.*, 2011), including algal and microbial mats that stabilize sediment, obstruct water movement and affect substrate elevation (Weerman *et al.*, 2010; Corenblit *et al.*, 2011; Da Lio *et al.*, 2013; Mariotti *et al.*, 2014). One such effect is where sediment accretion, promoted by mats, directs and enhances currents that cause scour and create channels (Bosak *et al.*, 2013a). Bosak *et al.* (2013b, fig. 5c) attributed closely spaced parallel 'corrugated' stromatolites, separated by 'gutters' in Marinoan cap carbonates (also see James *et al.*, 2001, figs 7c and d), to persistent erosion. Similarly, these authors attributed shapes of columns in the 750 to 800 Ma Upper Eleonore Bay Group, East Greenland to temporal and spatial patterns of increasing scour and shear (Bosak *et al.*, 2013a, fig. 5a). These astute assessments can also be applied at Tieling. The present authors infer that column width and spacing (i.e. runnel width) (Fig. 10) are self-organized responses to sediment-current/mat interactions.

Alignment

Alignment of Tieling stromatolite ridges and matrix-filled runnels suggests persistent current-swept, possibly tidal, conditions that transported carbonate mud, moulded ridges and scoured runnels. These elongate branched columns resemble other Proterozoic stromatolites thought to be aligned parallel to currents, for example, 1·9 Ga Pethei (Hoffman, 1989, fig. 8) and Rocknest (Grotzinger, 1989b, fig. 6) platforms and *ca* 0·9 to 1·0 Ga Glenelg/Aok Formation *Inzeria* stromatolites (Young, 1974; Young & Long, 1976). This suggests that Tieling columns and runnels could have been aligned parallel to prevailing current directions. However, other features suggest that Tieling columns may have developed normal to currents. In plan view, Tieling ridge–runnel patterns resemble symmetrical wave ripples and troughs in which the ripples (columns) tend to be less continuous and the troughs (runnels) are more continuous (Fig. 8A and B), and the ripples (columns) locally bifurcate. In some cases, however, the patterns appear inverse, with ridge/column plan more closely resembling that of ripple troughs, and runnel plan that of ripple crests (*cf.* Fig. 8 with Nienhuis *et al.*, 2014, fig. 1a). In addition, sloping (including sinuous) Tieling columns have laminae that tend to face in the direction of column inclination, suggesting accretion into the current (Tosti & Riding, 2016). In contrast, longitudinal sections, parallel to the ridge, are undulose to cuspate and relatively flat, with fewer truncation surfaces (Figs 7 and 12B). Tieling ridge–runnels also resemble much smaller patterns shown by *Kinneyia*, which Walcott (1914) thought might be cyanobacterial in origin. Biofilm growing under turbulent flow can develop ripple-like structures (Stoodley *et al.*, 1999) and Thomas *et al.* (2013) compared corrugations, induced normal to fluid flow in sheets of PVA film, with the surface pattern of *Kinneyia*, which typically have wavelengths of <2 cm. The type specimen of *Kinneyia* (Walcott, 1914) has a wavelength of *ca* 5 mm, whereas that of Tieling ridge–runnel systems is *ca* 5 to 10 cm. At Shark Bay, Mariotti *et al.* (2014) identified preferential mat colonization of sand bar runnels with wavelengths of 5 to 100 m. Although neither of these examples may be directly analogous to Tieling ridge–runnel systems, they demonstrate how physical conditions can influence linear patterns in mats and biofilm, and might indicate alignment normal to current and wave directions. These comparisons suggest that the axes of Tieling's distinctive ridge–runnel systems could have developed more or less normal to prevailing waves and/or current directions that scoured runnels and column margins, and transported carbonate mud. However, the possibility that Tieling ridge–runnels were aligned parallel to currents cannot be excluded. The present authors therefore conclude that Tieling ridge–runnel systems reflect self-organization with respect to currents and sediment supply, but whether stromatolite elongation was normal or parallel to these currents remains unresolved.

Coeval stromatolites in the Belt-Purcell Supergroup

Tieling (*ca* 1440 to 1400 Ma) stromatolites show similarities with well-documented examples of the same age in the Belt-Purcell succession of North America (Idaho, Montana, British Columbia and Alberta). The Belt-Purcell Supergroup is up to 20 km thick and *ca* 1470 to 1400 Ma in age (Evans *et al.*, 2000). The sediments are mainly siliciclastic, but stromatolite-bearing carbonates are present in the more shallow water north-eastern part of the outcrop in Glacier National Park and Waterton Lakes National Park where the succession is *ca* 3 km thick (Ross, 1959). Whether these deposits are marine or non-marine, or a mixture of both, has been debated for over a century. Fenton & Fenton (1937) considered the succession essentially marine. A non-marine origin, inferred by Walcott (1906, 1910), but subsequently abandoned by him (Fenton & Fenton, 1937), was revived by suggestions that the Belt-Purcell formed in an intracratonic rift setting (Winston, 1986, 1990, 2007; Sears, 2007). Marine conditions have been deduced from the presence of glauconite (Schieber, 1993) and geochemical data suggest that the Belt-Purcell was a marine basin that became isolated from the open ocean (Frank *et al.*, 1997; Luepke & Lyons, 2001). Its Proterozoic location near the western margin of Laurentia has suggested links with Australia (Karlstrom *et al.*, 2001), Siberia (Sears *et al.*, 2004, 2006) and North China (Su *et al.*, 2008).

In the area of Glacier National Park, the principal limestone–dolostone units are the Altyn, Helena/Siyeh and Shepard, plus thin carbonate horizons in shale-dominated units such as the Grinnell and Snowslip (Horodyski, 1989; Hunt, 2006). Stromatolites are present in all of these carbonates but are a minor component of the succession as a whole. For example, only 41 m of the 780 m thick Helena/Siyeh Formation in central Glacier National Park is stromatolitic (Horodyski, 1985, fig. 3). Belt-Purcell stromatolites nonetheless have a long history of research (Walcott, 1906, 1914; Fenton & Fenton, 1931, 1933, 1937; Rezak, 1957; White, 1970, 1984; Horodyski, 1975, 1976a,b, 1977, 1983, 1985, 1989). Prior to White (1970), who recognized *Baicalia*, Belt-Purcell stromatolites were generally described as species of *Collenia* and *Conophyton*. Horodyski (1976a) ascribed most Belt stromatolites that are circular in cross-section to either *Baicalia* or *Conophyton*, but also recognized *Jacutophyton*. 'Mound-shaped' stromatolites are relatively common in the Helena/Siyeh, Snowslip and Shepard formations (Horodyski, 1977, fig. 1). Two well-studied units with conical and/or columnar forms are the *Collenia columnaris* and *Collenia frequens* zones (Fenton & Fenton, 1931). The *Collenia columnaris* zone is in the upper Altyn. The *Collenia frequens* zone is a *ca* 30 m thick unit *ca* 200 m below the top of the Helena/Siyeh that is well-exposed near South Swiftcurrent Glacier (Horodyski, 1985, fig. 2). Rezak (1957) renamed elongate *Collenia* figured by Fenton & Fenton (1933, fig. 2) as *Conophyton inclinatum*, and termed the *Collenia* f*requens* zone the *Conophyton* 1 zone.

Vertical columns

Juxtaposed vertical columns similar to Tieling include the Altyn *Collenia columnaris* zone which Fenton & Fenton (1931, pl. 2, fig. 2) described as: "massive, light grey limestone in a single bed some 20 feet thick, and virtually, the entire mass of stone is formed by colonies of this one alga". For example, *Collenia columnaris* from near Mount Apikuni shows closely spaced columns, each about 15 cm wide (Fenton & Fenton, 1931, pl. 2). Similar forms occur in the Helena/Siyeh (Horodyski, 1977, fig. 5), some of which may be more longitudinal sections (Fenton & Fenton, 1937, pl. 18, fig. 2), and also slightly more divergent ones in the Altyn (Horodyski, 1977, fig. 6a, d). Passively branched forms in the upper Helena/Siyeh (Horodyski, 1976a, fig. 7) also resemble some Tieling examples in both column and lamina form.

Curved, sinusoidal forms

The Belt-Purcell contains examples of closely spaced columns that are curved to sinuous in vertical section and elongate in plan view, similar to those that occur in thin interbeds in the Old Quarry section (Tosti & Riding, 2016). Examples in the Altyn (e.g. Horodyski, 1983, fig. 4b, 5d-e) include columns inclined in different directions in subsequent beds (Horodyski, 1976b, fig. 5c) (evidently not heliotropic). Inclined and sinusoidal *Collenia columnaris* from the Altyn (Fenton & Fenton, 1937, pl. 9) closely resemble Tieling sinusoidal forms. Some are laterally very elongate (up to 80 cm in length, Fenton & Fenton, 1937, fig. 14b), similar to examples in the Tieling Roadside Section; they also occur in the Helena/Siyeh (Fenton &

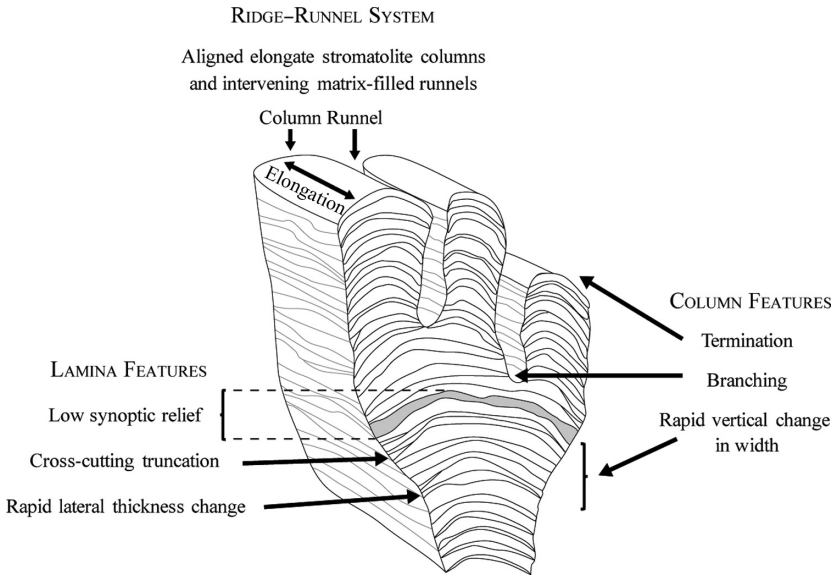

Fig. 21. Distinctive features of Tieling elongate columnar stromatolites: (i) Columns show marked vertical variation in width, frequent branching and terminations. (ii) Laminae show low synoptic relief, frequent cross-cutting truncations and rapid lateral changes in thickness. (iii) Ridge–runnel organization shows aligned elongate columns and narrow intervening matrix-filled runnels with signs of scour. In addition, primary microfabrics are fine-grained in both stromatolite and intervening matrix.

Fenton, 1937, pl. 18, fig. 1; Horodyski, 1977, fig. 4b; Horodyski, 1983, fig. 13e, 15a).

Truncated fine-grained lamina

Altyn stromatolites have fine-grained fabrics with truncated laminae that closely resemble Tieling examples. Horodyski (1976b, fig. 6) attributed truncations in Altyn columns to current erosion; White (1984, figs 4, 5) figured similar truncations in Altyn stratiform stromatolites. In a detailed examination of similar Altyn (Belt-Purcell) stromatolite fabrics, Horodyski (1976b, fig. 2a, b) interpreted 'finely (15 to 60 μm) crystalline dolomite pseudospar' as allochthonous and 'very finely (5 to 15 μm) crystalline dolomite pseudospar' as *in situ* precipitate. The present authors concur with this interpretation of trapping but see no evidence of precipitation and suggest that these differences are essentially neomorphic (see *Microfabric*, above). Furthermore, if precipitated layers were present, they probably would have noticeably affected column morphology. Therefore, it is suggested here that these Altyn fabrics are similar to Tieling and are products of stabilized and trapped sediment. This is consistent with the view that this general time period favoured the development of fine-agglutinated stromatolites (Fig. 20).

Recognition of fine-grained agglutinated stromatolites

Carbonate grain trapping and *in situ* precipitation are distinctly different processes of microbial carbonate formation (Awramik & Margulis, 1974; Burne & Moore, 1987; Dupraz *et al.*, 2009). However, many ancient fine-grained stromatolites have experienced some degree of alteration (Fairchild, 1991; Corkeron *et al.*, 2012). This can make it difficult to tell whether they originally consisted of trapped carbonate mud or microbial precipitated peloids and clotted fabrics, all of which are basically composed of relatively small grains (micrite, <4 μm) and crystals (microspar, 4 to 10 μm) (Horodyski, 1976b; Monty, 1976; Braithwaite *et al.*, 1989). Distinguishing these modes of formation in ancient stromatolites continues to challenge stromatolite research (Grotzinger & Knoll, 1999; Riding, 2000; Bosak *et al.*, 2013a).

Well-preserved Tieling stromatolites could shed light on this problem. They suggest that agglutinated stromatolites exhibit the following distinctive features, some of which are probably recognizable even in partly altered examples: (i) laminae with low synoptic relief; (ii) cross-cutting and truncated laminae with pronounced lateral changes in thickness; and (iii) columns that commonly branch, thicken and thin vertically, and show lateral migration. Tieling stromatolites also show textural similarity between stromatolite and matrix, both of which – where well-preserved – are very fine-grained.

In contrast, precipitated stromatolites are more likely to show the following: (i) either textural differences between stromatolite and matrix, or to lack matrix altogether; (ii) persistent laminae of relatively even thickness; (iii) enveloping laminae with high synoptic relief (but cf. Frantz *et al.*, 2015); (iv) relatively persistent column

width; and (v) rare or no branching (Riding, 1993). It is also possible that ridge–runnel organization, which is well-developed at Tieling, could be an additional feature characteristic of agglutinated stromatolites.

CONCLUSIONS

A key feature of Tieling stromatolites is that the primary microfabrics of both the columns and their adjacent matrix were essentially carbonate mud. The column sediment appears to have been cohesive rather than early lithified. Numerous fabric and morphological features support this interpretation and assist discrimination between agglutinated and precipitated stromatolites (Fig. 21). The laminae generally show low synoptic relief, rapid lateral change in thickness and frequent cross-cutting truncations. Marked variations in width accompany parallel to slightly divergent branching, and the columns also show frequent terminations. They form distinctive aligned systems of elongate ridge-like columns and adjacent scoured runnels. Mats colonized the sediment–water interface except where currents maintained intervening shallow runnels filled by carbonate mud plus small reworked mud flakes and silt-size grains. These features reflect interaction between copious current-borne sediment and microbial mats that, for the most part, coped with burial, recovered from frequent erosion and accreted quickly.

These well-preserved Mesoproterozoic stromatolites can be linked to the classic study by Black (1933) of cyanobacterial mats at Andros Island, and subsequent realization that bioturbation can hinder preservation of poorly lithified stromatolites (Shinn *et al.*, 1969; Garrett, 1970). Tieling stromatolites dominated shallow illuminated marine environments, and the pervasive ridge–runnel systems and well-developed planar bedding suggest relatively high-energy conditions. Their formation required several concurrent conditions, including: (i) copious supply of carbonate mud, thought to be a water column 'whiting' precipitate; (ii) mats composed of microbes such as multi-trichomous cyanobacteria able to trap this sediment, keep pace with its accretion and survive periodic burial; (iii) absence of significant early lithification; and (iv) lack of bioturbation. These conditions are consistent with Tieling's pre-animal age (Garrett, 1970), when Proterozoic carbonates were dominated more by allochthonous carbonate mud than by autochthonous sea floor precipitates (Grotzinger, 1989a, 1990; Knoll & Swett, 1990), and when filamentous cyanobacteria such as *Microcoleus* and *Schizothrix* had already evolved (Seong-Joo & Golubic, 1998) (Fig. 20).

A perennial question concerns the relative influence of environmental and biological factors on stromatolite shape. Tieling stromatolites evidently had essential biological requirements, such as suitable mat-forming microbes and lack of bioturbation, to promote their accretion and preservation. At the same time, they reflect specific environmental controls, such as abundant carbonate mud and persistent current effects that moulded the branched elongate column morphology. Yet another necessity, which may have been jointly mediated by environmental and biological processes, was mat surfaces that were cohesive rather than lithified, to promote trapping. Development of these deposits and their shapes therefore required specific organo-sedimentary feedbacks and interactions. The variety of morphotypes generated by these processes is mirrored in the taxonomic diversity of mid–late Proterozoic columnar stromatolites.

In addition to placing fine-grained agglutinated stromatolites in their environmental and secular perspectives, Tieling columns provide criteria to guide recognition of similar but less well-preserved examples; for example, low synoptic relief, numerous cross-cutting and truncated laminae with marked changes in thickness, rapid fluctuations in column width, frequent column branching and termination, and adjacent matrix similar in texture to the stromatolite columns. Conversely, they may also aid discrimination of precipitated stromatolite columns, which would probably show higher synoptic relief, more persistent enveloping laminae of relatively even thickness, less branching, gradual rather than rapid change in column width and textural contrasts between stromatolite and matrix, or lack of adjacent matrix altogether.

Aligned columnar stromatolite ridges and narrow intervening matrix-filled runnels appear to be quite common elsewhere in the mid–late Proterozoic. At Tieling, these are interpreted as a self-organized response to dynamic interaction between mat growth and copious current-borne sediment. In present-day examples, stromatolites can align parallel, but also normal, to current and wave directions. Comparisons with the alignment of associated cross-bedding and ripple marks that can change over short time-scales

may be misleading. The present authors favour the view that Tieling ridge–runnel systems were aligned normal to current/wave directions, similar to ripple patterns. However, at present, the possibility that they were aligned parallel to currents cannot be excluded. Textural and morphological similarities, including features indicative of fine-grained agglutination, between Tieling stromatolites and coeval examples in the Belt-Purcell Supergroup of Laurentia support the view that stromatolites can reflect time-limited conditions and biotas.

ACKNOWLEDGEMENTS

We are grateful to our field companions Liu Lijing and Li Yue; and also to Wu Yasheng for generously providing logistical support at Tieling. We thank Ted Labotka for help with XRD analyses, and Joe Panzik for advice on Nuna/Rodinia concepts. We are indebted to Aurélien Virgone for support and encouragement. Chen Meng-e kindly introduced RR to the Jixian Section in 1983. We thank Tracy Frank, Peir Pufahl, Elaine Richardson and Todd Boesiger for editing, and two anonymous reviewers for their helpful comments on the manuscript. This research was funded by TOTAL.

REFERENCES

Admiraal, W., **Peletier, H.** and **Zomer, H.** (1982) Observations and experiments on the population dynamics of epipelic diatoms from an estuarine mudflat. *Estuar. Coast. Shelf Sci.*, **14**, 471–487.

Altermann, W. (2008) Accretion, trapping and binding of sediment in Archean stromatolites—morphological expression of the antiquity of life. *Space Sci. Rev.*, **135**, 55–79.

Awramik, S.M. (1971) Precambrian columnar stromatolite diversity: reflection of metazoan appearance. *Science*, **174**, 825–827.

Awramik, S.M. and **Margulis, L.** (1974) *Stromatolite Newsletter*, **2**, 5.

Awramik, S.M. and **Riding, R.** (1988) Role of algal eukaryotes in subtidal columnar stromatolite formation. *Proc. Natl Acad. Sci. USA*, **85**, 1327–1329.

Awramik, S.M. and **Sprinkle, J.** (1999) Proterozoic stromatolites: the first marine evolutionary biota. *Hist. Biol.*, **13**, 241–253.

Berney, C. and **Pawlowski, J.** (2006) A molecular time-scale for eukaryote evolution recalibrated with the continuous microfossil record. *Proc. Roy. Soc. B*, **273**, 1867–1872.

Bernhard, J.M., **Edgcomb, V.P.**, **Visscher, P.T.**, **McIntyre-Wressnig, A.**, **Summons, R.E.**, **Bouxsein, M.L.**, **Louis, L.** and **Jeglinski, M.** (2013) Insights into foraminiferal influences on microfabrics of microbialites at Highborne Cay, Bahamas. *Proc. Natl Acad. Sci. USA*, **110**, 9830–9834.

Bertrand-Sarfati, J. (1976) An attempt to classify Late Precambrian stromatolite microstructure. In: *Stromatolites* (Ed. M.R. Walter), pp. 251–259. Elsevier, Amsterdam.

Bertrand-Sarfati, J. and **Awramik, S.M.** (1992) Stromatolites of the Mescal Limestone (Apache Group, middle Proterozoic, central Arizona): taxonomy, biostratigraphy, and paleoenvironments. *Geol. Soc. Am. Bull.*, **104**, 1138–1155.

Bertrand-Sarfati, J. and **Moussine-Pouchkine, A.** (1985) Evolution and environmental conditions of *Conophyton-Jacutophyton* associations in the Atar Dolomite (upper Proterozoic, Mauritania). *Precambrian Res.*, **29**, 207–234.

Black, M. (1933) The algal sedimentation of Andros Island Bahamas. Philosophical transactions of the Royal Society of London. *Series B Biological Sci.*, **222**, 165–192.

Blank, C.E. (2013) Origin and early evolution of photosynthetic eukaryotes in freshwater environments – reinterpreting Proterozoic paleobiology and biogeochemical processes in light of trait evolution. *J. Phycol.*, **49**, 1040–1055.

Blank, C.E. and **Sánchez-Baracaldo, P.** (2010) Timing of morphological and ecological innovations in the cyanobacteria – A key to understanding the rise in atmospheric oxygen. *Geobiology*, **8**, 1–23.

Bogdanova, S.V., **Pisarevsky, S.A.** and **Li, Z.X.** (2009) Assembly and Breakup of Rodinia (some results of IGCP Project 440). *Stratigr. Geol. Correl.*, **17**, 259–274.

Bosak, T., **Knoll, A.H.** and **Petroff, A.P.** (2013a) The meaning of stromatolites. *Annu. Rev. Earth Planet. Sci.*, **41**, 21–44.

Bosak, T., **Mariotti, G.**, **Macdonald, F.A.**, **Perron, J.T.** and **Pruss, S.B.** (2013b) Microbial sedimentology of stromatolites in Neoproterozoic cap carbonates. In: *Ecosystem Paleobiology and Geobiology, Paleontological Special Papers* (Eds A.M. Bush, S.B. Pruss and J.L. Payne), Paleontol. Soc., **19**, 51–77.

Braithwaite, C.J.R., **Casanova, J.**, **Frevert, T.** and **Whitton, B.A.** (1989) Recent stromatolites in landlocked pools on Aldabra, Western Indian Ocean. *Palaeogeogr. Palaeoclimatol. Palaeoecol.*, **69**, 145–165.

Browne, K.M., **Golubic, S.** and **Lee, S.-J.** (2000) Shallow marine microbial carbonate deposits. In: *Microbial Sediments* (Eds R. Riding and S.M. Awramik), pp. 233–249. Springer, Berlin.

Burne, R.V. and **Moore, L.** (1987) Microbialites; organosedimentary deposits of benthic microbial communities. *Palaios*, **2**, 241–254.

Butterfield, N.J., **Knoll, A.H.** and **Swett, K.** (1994) Paleobiology of the Upper Proterozoic Svanbergfjellet Formation, Spitsbergen. *Fossils Strata*, **34**, 1–84.

Cao, R.-J. and **Bian, L.-J.** (1985) An attempt to codify the morphological characteristic numbers of stromatolites. *Acta Palaeontogr. Sinica*, **24**, 629–634. (In Chinese with English table and abstract).

Cao, R.-J. and **Liang, Y.-Z.** (1974) On the classification and correlation of the Sinian System in China, based on a study of algae and stromatolites. Academia Sinica, *Nanking Inst. Geol. Palaeontol. Mem.*, **5**, 1–26. Science Press. In Chinese.

Cao, R.-J. and **Yuan, X.-L.** (2003) Pre-Sinian biostratigraphy of China. In: *Biostratigraphy of China* (Eds W.T. Zhang, P.-J. Chen and A.R. Palmer), pp. 1–29. Science Press, Beijing.

Carozzi, A.V. (1962) Cerebroid oolites. *Illinois State Acad. Sci. Trans.*, **55**, 239–249.

Castenholz, R.W. and **Garcia-Pichel, F.** (2012) Cyanobacterial responses to UV radiation. In: *Ecology of Cyanobacteria II, Their Diversity in Space and Time* (Ed. B.A. Whitton), pp. 481–499. Springer, Dordrecht, the Netherlands.

Chen, J.-B., **Zhang, H.-M.**, **Zhu, S.-X.**, **Zhao, Z.** and **Wang, Z.-G.** (1980) Research on Sinian Suberathem of Jixian, Tianjin. In: *Research on Precambrian geology, Sinian Suberathem in China* (Eds Tianjin Institute of Geology and Mineral Resources, Chinese Academy of Geological Sciences), pp. 56–114. Tianjin Science and Technology Press, Tianjin (In Chinese, with English abstract.)

Chen, J., **Zhang, H.**, **Xing, Y.** and **Ma, G.** (1981) On the upper Precambrian (Sinian Suberathem) in China. *Precambrian Res.*, **15**, 207–228.

Chen, L., **Huang, B.**, **Yi, Z.**, **Zhao, J.** and **Yan, Y.** (2013) Paleomagnetism of ca. 1.35 Ga sills in northern North China Craton and implications for paleogeographic reconstruction of the Mesoproterozoic supercontinent. *Precambrian Res.*, **228**, 36–47.

Chu, X., **Zhang, T.**, **Zhang, Q.** and **Lyons, T.W.** (2007) Sulfur and carbon isotope records from 1700 to 800 Ma carbonates of the Jixian section, northern China: Implications for secular isotope variations in Proterozoic seawater and relationships to global supercontinental events. *Geochim. Cosmochim. Acta*, **71**, 4668–4692.

Cloud, P.E., Jr and **Barnes, V.E.** (1948) The Ellenburger group of central Texas. *Bur. Econ. Geol. Univ. Tex.* Publication, **4621**, 1–473, 45 pls.

Coco, G. and **Murray, A.B.** (2007) Patterns in the sand: from forcing templates to self-organization. *Geomorphology*, **91**, 271–290.

Corenblit, D., **Baas, A.C.**, **Bornette, G.**, **Darrozes, J.**, **Delmotte, S.**, **Francis, R.A.**, **Gurnell, A.M.**, **Julien, F.**, **Naiman, R.J.** and **Steiger, J.** (2011) Feedbacks between geomorphology and biota controlling Earth surface processes. *Earth-Sci. Rev.*, **106**, 307–331.

Corkeron, M., **Webb, G.E.**, **Moulds, J.** and **Grey, K.** (2012) Discriminating stromatolite formation modes using rare earth element geochemistry: trapping and binding versus in situ precipitation of stromatolites from the Neoproterozoic Bitter Springs Formation, Northern Territory, Australia. *Precambrian Res.*, **212–213**, 194–206.

Cozzi, A., **Grotzinger, J.P.** and **Allen, P.A.** (2004) Evolution of a terminal Neoproterozoic carbonate ramp system (Buah Formation, Sultanate of Oman): effects of basement paleotopography. *Geol. Soc. Am. Bull.*, **116**, 1367–1384.

Da Lio, C., **D'Alpaos, A.** and **Marani, M.** (2013) The secret gardener: vegetation and the emergence of biogeomorphic patterns in tidal environments. *Phil. Trans. R Soc. A*, **371**, 20120367.

Dill, R.F., **Shinn, E.A.**, **Jones, A.T.**, **Kelly, K.** and **Steinen, R.P.** (1986) Giant subtidal stromatolites forming in normal salinity waters. *Nature*, **324**, 55–58.

Dupraz, C., **Reid, R.P.**, **Braissant, O.**, **Decho, A.W.**, **Norman, R.S.** and **Visscher, P.T.** (2009) Processes of carbonate precipitation in modern microbial mats. *Earth-Sci. Rev.*, **96**, 141–162.

Dyer, K.R. and **Huntley, D.A.** (1999) The origin, classification and modelling of sand banks and ridges. *Cont. Shelf Res.*, **19**, 1285–1330.

Eardley, A.J. (1938) Sediments of Great Salt Lake, Utah. *AAPG Bull.*, **22**, 1305–1411.

Ernst, R.E., **Bleeker, W.**, **Söderlund, U.** and **Kerr, A.C.** (2013) Large Igneous Provinces and supercontinents: toward completing the plate tectonic revolution. *Lithos*, **174**, 1–14.

Erwin, D.H., **Laflamme, M.**, **Tweedt, S.M.**, **Sperling, E.A.**, **Pisani, D.** and **Peterson, K.J.** (2011) The Cambrian conundrum: early divergence and later ecological success in the early history of animals. *Science*, **334**, 1091–1097.

Evans, D.A.D. (2013) Reconstructing pre-Pangean supercontinents. *Geol. Soc. Am. Bull.*, **125**, 1735–1751.

Evans, K.V., **Aleinikoff, J.N.**, **Obradovich, J.D.** and **Fanning, C.M.** (2000) SHRIMP U-Pb geochronology of volcanic rocks, Belt Supergroup, western Montana: evidence for rapid deposition of sedimentary strata. *Can. J. Earth Sci.*, **37**, 1287–1300.

Fairchild, I.J. (1991) Origins of carbonate in Neoproterozoic stromatolites and the identification of modern analogues. *Precambrian Res.*, **53**, 281–299.

Fenton, C.L. and **Fenton, M.A.** (1931) Algae and algal beds in the Belt Series of Glacier National Park. *J. Geol.*, **39**, 670–686.

Fenton, C.L. and **Fenton, M.A.** (1933) Algal reefs or bioherms in the Belt Series of Montana. *Geol. Soc. Am. Bull.*, **44**, 1135–1142, 1 pl.

Fenton, C.L. and **Fenton, M.A.** (1937) Belt Series of the north: stratigraphy, sedimentation, paleontology. *Geol. Soc. Am. Bull.*, **48**, 1873–1970.

Frank, T.D., **Lyons, T.W.** and **Lohmann, K.C.** (1997) Isotopic evidence for the paleoenvironmental evolution of the Mesoproterozoic Helena Formation (Belt Supergroup, Montana). *Geochim. Cosmochim. Acta*, **61**, 5023–5041.

Frantz, C.M., **Petryshyn, V.A.** and **Corsetti, F.A.** (2015) Grain trapping by filamentous cyanobacterial and algal mats: implications for stromatolite microfabrics through time. *Geobiology*, **13**, 409–423.

Gao, Z.-X., **Xung, Y.-X.** and **Gao, P.** (Kao, C.S., Hsiung, Y.H. and Kao, P.), (1934) Preliminary notes on Sinian stratigraphy of North China. *Geol. Soc. China Bull.*, **13**, 243–287.

Gao, L.Z., **Zhang, C.H.**, **Shi, X.Y.**, **Zhou, H.R.** and **Wang, Z.Q.** (2007) Zircon SHRIMP U-Pb dating of the tuff bed in the Xiamaling Formation of the Qingbaikou System in North China. *Geol. Bull. China*, **26**, 249–255.

Gao, L.Z., **Zhang, C.H.**, **Shi, X.Y.**, **Song, B.**, **Wang, Z.Q.** and **Liu, Y.M.** (2008) Mesoproterozoic age for Xiamaling Formation in North China plate indicated by zircon SHRIMP dating. *Chinese Sci. Bull.*, **53**, 2665–2671.

Garrett, P. (1970) Phanerozoic Stromatolites: noncompetitive ecologic restriction by grazing and burrowing animals. *Science*, **169**, 171–173.

Gebelein, C.D. (1969) Distribution, morphology, and accretion rate of recent subtidal algal stromatolites, Bermuda. *J. Sed. Petrol.*, **39**, 49–69.

Gerdes, G., **Klenke, T.** and **Noffke, N.** (2000) Microbial signatures in peritidal siliciclastic sediments: a catalogue. *Sedimentology*, **47**, 279–308.

Ginsburg, R.N. and **Lowenstam, H.A.** (1958) The influence of marine bottom communities on the depositional environment of sediments. *J. Geol.*, **66**, 310–318.

Ginsburg, R.N., **Isham, L.B.**, **Bein, S.J.** and **Kuperberg, J.** (1954) Laminated algal sediments of South Florida and their recognition in the fossil record. Marine Laboratory, University of Miami, Coral Gables, Florida, Unpublished Report, 54-20, 33 pp.

Glaessner, M.F., **Preiss, W.V.** and **Walter, M.R.** (1969) Precambrian columnar stromatolites in Australia:

morphological and stratigraphic analysis. *Science*, **164**, 1056–1058.

Goldring, W. (1938) Algal barrier reefs in the Lower Ozarkian of New York with a chapter on the importance of coralline algae as reef builders through time. *New York State Museum Bull.*, **315**, 5–75.

Gorokhov, I.M., **Semikhatov, M.A.**, **Arakelyants, M.M.**, **Fallick, E.A.**, **Melnikova, N.N.**, **Turchenko, T.L.**, **Ivanovskaya, T.A.**, **Zaitseva, T.S.** and **Kutyavin, E.P.** (2006) Rb–Sr, K-Ar, H- and O-isotope systematics of the Middle Riphean shales from the Debengda Formation, the Olenek Uplift, North Siberia. *Stratigr. Geol. Correl.*, **14**, 260–274.

Grotzinger, J.P. (1989a) Facies and evolution of Precambrian carbonate depositional systems: emergence of the modern platform archetype. In: *Controls on Carbonate Platform and Basin Development* (Eds P.D. Crevello, J.L. Wilson, J.F. Sarg and J.F. Read), SEPM Spec. Publ., **44**, 79–106.

Grotzinger, J.P. (1989b) Construction of early Proterozoic (1.9 Ga) barrier reef complex, Rocknest Platform, Coronation Gulf, Northwest Territories. In: *Reefs, Canada and Adjacent Area* (Eds H.H.J. Geldsetzer, N.P. James and G.E. Tebbutt). Can. Soc. Petrol. Geol. Memoir., **13**, 30–37.

Grotzinger, J.P. (1990) Geochemical model for Proterozoic stromatolite decline. *Am. J. Sci.*, **290-A**, 80–103.

Grotzinger, J.P. (1994) Trends in Precambrian carbonate sediments and their implication for understanding evolution. In: *Early life on Earth: Nobel Symposium 84* (Ed. S. Bengtson), pp. 245–258. Columbia University Press, New York.

Grotzinger, J.P. and **Kasting, J.F.** (1993) New constraints on Precambrian ocean composition. *J. Geol.*, **101**, 235–243.

Grotzinger, J.P. and **Knoll, A.H.** (1999) Stromatolites in Precambrian carbonates: evolutionary mileposts or environmental dipsticks? *Annu. Rev. Earth Planet. Sci.*, **27**, 313–358.

Guo, H., **Du, Y.**, **Kah, L.C.**, **Huang, J.-H.**, **Hu, C.-Y.**, **Huang, H.** and **Yu, W.-C.** (2013) Isotopic composition of organic and inorganic carbon from the Mesoproterozoic Jixian Group, North China: implications for biological and oceanic evolution. *Precambrian Res.*, **224**, 169–183.

Halfen, L.N. and **Castenholz, R.W.** (1971) Gliding motility in the blue- green alga *Oscillatoria princeps*. *J. Phycol.*, **7**, 133–145.

Hardie, L.A. (1977) *Sedimentation on the Modern Carbonate Tidal Flats of Northwest Andros Island, Bahamas: the Johns Hopkins University Studies in Geology*. The Johns Hopkins University Press, Baltimore, 224 pp.

Harris, P.M., **Purkis, S.J.** and **Ellis, J.** (2011) Analyzing spatial patterns in modern carbonate sand bodies from Great Bahama Bank. *J. Sed. Res.*, **81**, 185–206.

Haslett, P.G. (1976) Lower Cambrian stromatolites from open and sheltered intertidal environments, Wirrealpa, South Australia. In: *Stromatolites* (Ed. M.R. Walter), *Developments in Sedimentology*, **20**, pp. 565–584. Elsevier, Amsterdam.

Herrington, P.M. and **Fairchild, I.J.** (1989) Carbonate shelf and slope facies evolution prior to Vendian glaciation, central East Greenland. In: *The Caledonide Geology of Scandinavia* (Ed. R.A. Gayer), pp. 263–273. Graham and Trotman, London.

Hoffman, P.F. (1967) Algal stromatolites: use in stratigraphic correlation and paleocurrent determination. *Science*, **157**, 1043–1045.

Hoffman, P.F. (1976a) Environmental diversity of middle Precambrian stromatolites. In: *Stromatolites* (Ed. M.R. Walter), *Developments in Sedimentology*, **20**, pp. 599–611. Elsevier, Amsterdam.

Hoffman, P.F. (1976b) Stromatolite morphogenesis in Shark Bay, Western Australia. In: *Stromatolites* (Ed. M.R. Walter), *Developments in Sedimentology*, **20**, pp. 261–271. Elsevier, Amsterdam.

Hoffman, P.F. (1989) Pethei reef complex (1.9 Ga), Great Slave Lake, N.W.T. In: *Reefs, Canada and Adjacent Area* (Eds H.H.J. Geldsetzer, N.P. James and G.E. Tebbutt). *Canadian Society of Petroleum Geologists, Memoir*, **13**, 38–48.

Hoffman, P.F. and **Halverson, G.P.** (2011) Neoproterozoic glacial record in the Mackenzie Mountains, northern Canadian Cordillera. In: *The Geological Record of Neoproterozoic Glaciations* (Eds E. Arnaud, G.P. Halverson and G. Shields-Zhou), pp. 397–412. The Geological Society, London.

Holland, K.T. and **Elmore, P.A.** (2008) A review of heterogeneous sediments in coastal environments. *Earth-Sci. Rev.*, **89**, 116–134.

Horodyski, R.J. (1975) Stromatolites of the lower Missoula Group (Middle Proterozoic), Belt Supergroup, Glacier National Park, Montana. *Precambrian Res.*, **2**, 215–254.

Horodyski, R.J. (1976a) Stromatolites of the upper Siyeh Limestone (Middle Proterozoic), Belt Supergroup, Glacier National Park, Montana. *Precambrian Res.*, **3**, 517–536.

Horodyski, R.J. (1976b) Stromatolites from the middle Proterozoic Altyn Limestone, Belt Supergroup, Glacier National Park, Montana. In: *Stromatolites* (Ed. M.R. Walter). *Developments in Sedimentology*, **20**, pp. 585–597. Elsevier, Amsterdam.

Horodyski, R.J. (1977) Environmental influences on columnar stromatolite branching patterns: examples from the Middle Proterozoic Belt Supergroup, Glacier National Park, Montana. *J. Paleontol.*, **51**, 661–671.

Horodyski, R.J. (1983) Sedimentary geology and stromatolites of the middle Proterozoic Belt Supergroup, Glacier National Park, Montana. *Precambrian Res.*, **20**, 391–425.

Horodyski, R.J. (1985) Stromatolites of the Middle Proterozoic Belt Supergroup, Glacier National Park, Montana: summary and a comment on the Relationships between their Morphology and Paleoenvironment. In: *Paleoalgology: contemporary Research and Applications* (Eds D.F. Toomey and M.H. Nitecki), pp. 34–39. Springer, Berlin-Heidelberg.

Horodyski, R.J. (1989) Stromatolites of the Belt Supergroup, Glacier National Park, Montana. In: *Middle Proterozoic Belt Supergroup, western Montana. 28th International Geological Congress, Field Trip Guidebook T334* (Eds D. Winston, R.J. Horodyski and J.W. Whip), pp. 27–45. American Geophysical Union, Washington, D.C.

Hunt, R. (2006) Middle Proterozoic paleontology of the Belt Supergroup, Glacier National Park. In: *Fossils from Federal Lands* (Eds S.G. Lucas, J.A. Spielmann, P.M. Hester, J.P. Kenworthy and V.L. Santucci). New Mex. Museum Nat. Hist. Sci. Bull., **34**, 57–62.

Hunter, R.E. (1969) Eolian microridges on modern beaches and a possible ancient example. *J. Sed. Petrol.*, **39**, 1573–1578.

Hunter, R.E. (1973) Pseudo-crosslamination formed by climbing adhesion ripples. *J. Sed. Petrol.*, **43**, 1125–1127.

James, N.P., **Narbonne, G.M.** and **Kyser, T.K.** (2001) Late Neoproterozoic cap carbonates: mackenzie Mountains, northwestern Canada: precipitation and global glacial meltdown. *Can. J. Earth Sci.*, **38**, 1229–1262.

Jørgensen, B.B., **Cohen, Y.** and **Revsbech, N.P.** (1986) Transition from anoxygenic to oxygenic photosynthesis in a Microcoleus chthonoplastes cyanobacterial mat. *Appl. Environ. Microbiol.*, **51**, 408–417.

Jørgensen, B.B., **Cohen, Y.** and **Revsbech, N.P.** (1988) Photosynthetic potential and light-dependent oxygen consumption in a benthic cyanobacterial mat. *Appl. Environ. Microbiol.*, **54**, 176–182.

Kah, L.C. and **Grotzinger, J.P.** (1992) Early Proterozoic (1.9 Ga) thrombolites of the Rocknest Formation, Northwest Territories, Canada. *Palaios*, **7**, 305–315.

Kah, L.C. and **Knoll, A.H.** (1996) Microbenthic distribution of Proterozoic tidal flats: environmental and taphonomic considerations. *Geology*, **24**, 79–82.

Kah, L.C. and **Riding, R.** (2007) Mesoproterozoic carbon dioxide levels inferred from calcified cyanobacteria. *Geology*, **35**, 799–802.

Kalkowsky, E. (1908) Oölith und Stromatolith im norddeutschen Buntsandstein. *Z. Deut. Geol. Ges.*, **60**, 68–125, 4–11 pls.

Karlstrom, K.E., **Ahall, K.I.**, **Harlan, S.S.**, **Williams, M.L.**, **McLelland, J.** and **Geissman, J.W.** (2001) Long-lived (1.8–1.0 Ga) convergent margin in southern Laurentia, its extensions to Australia and Baltica, and implications for refining Rodinia. *Precambrian Res.*, **111**, 5–30.

Kirwan, M.L. and **Murray, A.B.** (2007) A coupled geomorphic and ecological model of tidal marsh evolution. *Proc. Natl Acad. Sci. USA*, **104**, 6118–6122.

de Klein, G. (1970) Depositional and dispersal dynamics of intertidal sand bars. *J. Sed. Petrol.*, **40**, 1095–1127.

Knoll, A.H. (2014) Paleobiological perspectives on early eukaryotic evolution. *Cold Spring Harb. Perspect. Biol.*, **6**, p.a016121.

Knoll, A.H. and **Swett, K.** (1990) Carbonate deposition during the late Proterozoic Era: an example from Spitsbergen. *Am. J. Sci.*, **290A**, 104–132.

Knoll, A.H., **Swett, K.** and **Burkhardt, E.** (1989) Paleoenvironmental distribution of microfossils and stromatolites in the upper Proterozoic Backlundtoppen Formation, Spitsbergen. *J. Paleontol.*, **63**, 129–145.

Knoll, A.H., **Wörndle, S.** and **Kah, L.C.** (2013) Covariance of microfossil assemblages and microbialite textures across an Upper Mesoproterozoic carbonate platform. *Palaios*, **28**, 453–470.

Kocurek, G. and **Fielder, G.** (1982) Adhesion structures. *J. Sed. Petrol.*, **52**, 1229–1241.

Korolyuk, I.K. (1963) Stromatolites of the late Precambrian. In: *Stratigrafiya SSSR, Verkhnii Dokembrii.* (Ed. B.M. Keller), pp. 479–498. Gosgeoltekhizdat, Moscow (in Russian).

Kromkamp, J.C., **Perkins, R.**, **Dijkman, N.**, **Consalvey, M.**, **Andres, M.** and **Reid, R.P.** (2007) Resistance to burial of cyanobacteria in stromatolites. *Aquat. Microbial Ecol.*, **48**, 123–130.

Li, H.K., **Lu, S.N.**, **Li, H.M.**, **Sun, L.X.**, **Xiang, Z.Q.**, **Geng, J.Z.** and **Zhou, H.Y.** (2009) Zircon and beddeleyite U-Pb precision dating of basic rock sills intruding Xiamaling Formation, North China. *Geol. Bull. China*, **28**, 1396–1404.

Li, H.K., **Zhu, S.X.**, **Xiang, Z.Q.**, **Su, W.B.**, **Lu, S.N.**, **Zhou, H.Y.**, **Geng, J.Z.**, **Li, S.** and **Yang, F.J.** (2010) Zircon U-Pb dating on tuff bed from Gaoyuzhuang Formation in Yanqing, Beijing: further constraints on the new subdivision of the Mesoproterozoic stratigraphy in the northern North china craton. *Acta Petrologica Sinica*, **26**, 2131–2140.

Li, H., **Lu, S.**, **Su, W.**, **Xiang, Z.**, **Zhou, H.** and **Zhang, Y.** (2013) Recent advances in the study of the Mesoproterozoic geochronology in the North China Craton. *J. Asian Earth Sci.*, **72**, 216–227.

Li, H.K., **Su, W.B.**, **Zhou, H.Y.**, **Xiang, Z.Q.**, **Tian, H.**, **Yang, L.G.**, **Huff, W.D.** and **Ettensohn, F.R.** (2014) The first precise age constraints on the Jixian System of the Meso- to Neoproterozoic standard section of China: SHRIMP zircon U-Pb dating of bentonites from the Wumishan and Tieling formations in the Jixian section, North China Craton. *Acta Petrologica Sinica*, **30**, 2999–3012. In Chinese, with English abstract.

Logan, B.W. (1961) *Cryptozoon* and associated stromatolites from the Recent, Shark Bay, Western Australia. *J. Geol.*, **69**, 517–533.

Logan, B.W. and **Semeniuk, V.** (1976) Dynamic metamorphism: processes and products in Devonian carbonate rocks, Canning Basin, Western Australia. *Geol. Soc. Aust. Spec. Pub.*, **6**, 138.

Lu, S.N. (1992) Chronology of Jixian Section of Middle-Upper Proterozoic strata. In: *Symposium of Research on Modern Geology*, pp. 122–129. (Eds Q.B. Li, J.X. Dai, R.Q. Liu and J.L. Li), Nanjing University Press, Nanjing. (in Chinese with English abstract).

Lu, S.N., **Zhao, G.C.**, **Wang, H.M.** and **Hao, G.J.** (2008) Precambrian metamorphic basement and sedimentary cover of the North China Craton: a review. *Precambrian Res.*, **160**, 77–93.

Luepke, J.J. and **Lyons, T.W.** (2001) Pre-Rodinian (Mesoproterozoic) supercontinental rifting along the western margin of Laurentia: geochemical evidence from the Belt-Purcell Supergroup. *Precambrian Res.*, **111**, 79–90.

Maloof, A.C. and **Grotzinger, J.P.** (2012) The Holocene shallowing-upward parasequence of north-west Andros Island, Bahamas. *Sedimentology*, **59**, 1375–1407.

Mariotti, G., **Perron, J.T.** and **Bosak, T.** (2014) Feedbacks between flow, sediment motion and microbial growth on sandbars initiate and shape elongated stromatolite mounds. *Earth Planet. Sci. Lett.*, **397**, 93–100.

Maslov, V.P. (1961) Algae and carbonate deposition. Izv. Akad. Nauk SSSR. *Ser. Geol.*, **12**, 81–86. (in Russian).

Meert, J.G. and **Powell, C.M.A** (2001) Assembly and break–up of Rodinia: introduction to the special volume. *Precambrian Res.*, **110**, 1–8.

Mei, M., **Yang, F.**, **Gao, J.** and **Meng, Q.** (2008) Glauconites formed in the high-energy shallow-marine environment of the Late Mesoproterozoic: case study from Tieling Formation at Jixian Section in Tianjin, North China. *Earth Sci. Front.*, **15**, 146–158.

Meng, Q.-R., **Wei, H.-H.**, **Qu, Y.-Q.** and **Ma, S.-X.** (2011) Stratigraphic and sedimentary records of the rift to drift evolution of the northern North China craton at the Paleo- to Mesoproterozoic transition. *Gondwana Res.*, **20**, 205–218.

Monty, C. (1965) Recent algal stromatolites in the Windward lagoon, Andros Island, Bahamas. *Ann. Soc Géol. Belg.*, **88**, 269–276.

Monty, C. (1972) Recent algal stromatolitic deposits, Andros Island Bahamas. *Preliminary Rep. Geologische Rundschau*, **61**, 742–783.

Monty, C. (1976) The origin and development of cryptalgal fabrics. In: *Stromatolites.* (Ed. M.R. Walter). *Developments in Sedimentology,* **20**, pp. 193–249. Elsevier, Amsterdam.

Monty, C.L.V. and **Hardie, L.A.** (1976) *The geological significance of the freshwater blue-green algal calcareous*

marsh. In: *Stromatolites*. (Ed. M.R. Walter), *Developments in Sedimentology*, *20*, pp. 447–477. Elsevier, Amsterdam.

Moon, Y.-J., **Kim, S.I.** and **Chung, Y.-H.** (2012) Sensing and responding to UV-A in cyanobacteria. *Int. J. Mol. Sci.*, **13**, 16303–16332. doi:10.3390/ijms131216303.

Nienhuis, J.H., **Perron, J.T.**, **Kao, J.C.T.** and **Myrow, P.M.** (2014) Wavelength selection and symmetry breaking in orbital wave ripples. *J. Geophys. Res. Earth Surface*, **119**, 2239–2257.

Paull, C.K., **Neumann, A.C.**, **Bebout, B.**, **Zabielski, V.** and **Showers, W.** (1992) Growth rate and stable isotopic character of modern stromatolites from San Salvador, Bahamas. *Palaeogeogr. Palaeoclimatol. Palaeoecol.*, **95**, 335–344.

Pelechaty, S.M. and **Grotzinger, J.P.** (1989) Stromatolite bioherms of a 1.9 Ga foreland basin carbonate ramp, Beechey Formation, Kilohigok Basin, Northwest Territories. In: *Reefs of Canada and Adjacent Areas* (Eds H.H.J. Geldsetzer, N.P. James and E. Tebbutt). Can. Soc. Pet. Geol. Mem., **13**, 49–54.

Pentecost, A. (1984) Effects of sedimentation and light intensity on mat-forming Oscillatoriaceae with particular reference to *Microcoleus lyngbyaceus* Gomont. *J. Gen. Microbiol.*, **130**, 983–990.

Perry, C.T., **Salter, M.A.**, **Harborne, A.R.**, **Crowley, S.F.**, **Jelks, H.L.** and **Wilson, R.W.** (2011) Fish as major carbonate mud producers and missing components of the tropical carbonate factory. *Proc. Natl Acad. Sci. USA*, **108**, 3865.

Pesonen, L.J., **Mertanen, S.** and **Veikkolainen, T.** (2012) Paleo-Mesoproterozoic supercontinents — a paleomagnetic view. *Geophysica*, **48**, 5–47.

Pisarevsky, S.A., **Elming, S.A.**, **Pesonen, L.J.** and **Li, Z.-X.** (2014) Mesoproterozoic paleogeography: Supercontinent and beyond. *Precambrian Res.*, **244**, 207–225.

Playford, P.E. and **Cockbain, A.E.** (1976) Modern algal stromatolites at Hamelin Pool, a hypersaline barred basin in Shark Bay, Western Australia. In: *Stromatolites*, pp. 389–411. (Ed. M.R. Walter), Elsevier, Amsterdam.

Porter, S.M. and **Knoll, A.H.** (2000) Testate amoebae in the Neoproterozoic era: evidence from vase-shaped microfossils in the Chuar Group, Grand Canyon. *Paleobiology*, **26**, 360–385.

Preiss, W.V. (1972) The systematics of South Australian Precambrian and Cambrian stromatolites, Part 1. *Trans. Roy. Soc. S. Aust.*, **96**, 67–100.

Qian, X. (1985) Late Precambrian aulacogens of the North China Craton. Conference on Terrestrial Planets: Comparative Planetology, June 5-7, 1985, California Institute of Technology, Pasadena, CA, abstracts, pp. 115–117. LPI Contribution 575, published by the Lunar and Planetary Institute, 3303 Nasa Road 1, Houston, TX 77058.

Qu, Y., **Pan, J.**, **Ma, S.**, **Lei, Z.**, **Li, L.** and **Wu, G.** (2014) Geological characteristics and tectonic significance of unconformities in Mesoproterozoic successions in the northern margin of the North China Block. *Geosci. Frontiers*, **5**, 127–138.

Raaben, M.E. (1969) Columnar stromatolites and late Precambrian stratigraphy. *Am. J. Sci.*, **267**, 1–18.

Raaben, M.E., **Sinha, A.K.** and **Sharma, M.** (2001) *Precambrian stromatolites of India and Russia*. Birbal Sahni Institute of Palaeobotany, Lucknow, India.

Rankey, E.C. and **Berkeley, A.** (2012) Holocene carbonate tidal flats. In: *Principles of Tidal Sedimentology* (Eds R.A. Davis Jr and R.W. Dalrymple), pp. 507–535. Springer, Dordrecht.

Rankey, E.C., **Riegl, B.** and **Steffen, K.** (2006) Form, function and feedbacks in a tidally dominated ooid shoal, Bahamas. *Sedimentology*, **53**, 1191–1210.

Reid, R.P., **Visscher, P.T.**, **Decho, A.W.**, **Stolz, J.F.**, **Bebout, B.M.**, **Dupraz, C.**, **Macintyre, I.G.**, **Paerl, H.W.**, **Pinckney, J.L.**, **Prufert-Bebout, L.**, **Steppe, T.F.** and **DesMarais, D.J.** (2000) The role of microbes in accretion, lamination and early lithification of modern marine stromatolites. *Nature*, **406**, 989–992.

Rezak, R. (1957) Stromatolites of the Belt Series in Glacier National Park and vicinity, Montana. *U.S. Geol. Surv. Prof. Pap.*, **294-D**, 127–154.

Ricketts, B.D. (1983) The evolution of a middle Precambrian dolostone sequence – a spectrum of dolomitization regimes. *J. Sed. Petrol.*, **53**, 565–586.

Riding, R. (1991) Classification of microbial carbonates. In: *Calcareous Algae and Stromatolites* (Ed. R. Riding), pp. 21–51. Springer-Verlag, Berlin.

Riding, R. (1993) Interaction between accretionary process, relative relief, and external shape in stromatolites and related microbial deposits. International Alpine Algae Symposium and Field Meeting, Munich-Vienna, 29 August-5 September 1993, Abstracts.

Riding, R. (2000) Microbial carbonates: the geological record of calcified bacterial-algal mats and biofilms. *Sedimentology*, **47** (Suppl 1), 179–214.

Riding, R. (2006) Cyanobacterial calcification, carbon dioxide concentrating mechanisms, and Proterozoic-Cambrian changes in atmospheric composition. *Geobiology*, **4**, 299–316.

Roberts, N.M.W. (2013) The boring billion? Lid tectonics, continental growth and environmental change associated with the Columbia supercontinent. *Geosci. Frontiers*, **4**, 681–691.

Rogers, J.J.W. and **Santosh, M.** (2002) Configuration of Columbia, a Mesoproterozoic Supercontinent. *Gondwana Res.*, **5**, 5–22.

Ross, C.P. (1959) Geology of Glacier National Park and the Flathead region, northwestern Montana. *U.S. Geol. Surv. Prof. Pap.*, **296**, 125.

Round, F.E. (1971) Benthic marine diatoms. *Oceanogr. Mar. Biol. Annu. Rev.*, **9**, 83–139.

Ruppel, S.C. and **Kerans, C.** (1987) Paleozoic buildups and associated facies, Llano Uplift, Central Texas. *Aust. Geol. Soc. Guidebook*, **10**, 33.

Sami, T.T. and **James, N.P.** (1993) Evolution of an early Proterozoic foreland basin carbonate platform, lower Pethei Group, Great Slave Lake, north-west Canada. *Sedimentology*, **40**, 403–430.

Sánchez-Baracaldo, P., **Ridgwell, A.** and **Raven, J.A.** (2014) A Neoproterozoic transition in the marine nitrogen cycle. *Curr. Biol.*, **24**, 652–657.

Santosh, M., **Zhao, D.P.** and **Kusky, T.M.** (2010) Mantle dynamics of the Paleoproterozoic North China Craton: a perspective based on seismic tomography. *J. Geodynamics*, **49**, 39–53.

Schieber, J. (1993) Sedimentologic, geochemical, and mineralogical features of the Belt Supergroup and their bearing on the lacustrine versus marine debate. In: *Proceedings of the Belt Symposium III: Montana Bureau of Mines and Geology* (Ed. R.B. Berg), Spec. Publ., **112**, 177–189.

Sears, J.W. (2007) Belt-Purcell Basin: keystone of the Rocky Mountain fold-and-thrust belt, United States and Canada. *Geol. Soc. Am. Spec. Pap.*, **433**, 147–166.

Sears, J.W., **Price, R.A.** and **Khudoley, A.K.** (2004) Linking the Mesoproterozoic Belt-Purcell and Udzha basins across the west Laurentia-Siberia connection. *Precambrian Res.*, **129**, 291–308.

Sears, J.W., **Price, R.A.** and **Khudoley, A.K.** (2006) Reply to the comment by Natapov *et al.* (2005) on Linking the Mesoproterozoic Belt-Purcell and Udzha basins across the west Laurentia-Siberia connection [Precambrian Res. 129 (2004) 291–308]. *Precambrian Res.*, **145**, 157–158.

Seong-Joo, L. and **Golubic, S.** (1998) Multi-trichomous cyanobacterial microfossils from the Mesoproterozoic Gaoyuzhuang Formation, China: paleoecological and taxonomic implications. *Lethaia*, **31**, 169–184.

Seong-Joo, L., **Browne, K.M.** and **Golubic, S.** (2000) On stromatolite lamination. In: *Microbial sediments* (Eds R. Riding and S.M. Awramik), pp. 16–24. Springer, Berlin.

Serebryakov, S.N. (1976) Biotic and abiotic factors controlling the morphology of Riphean stromatolites. In: *Stromatolites* (Ed. M.R. Walter), *Developments in Sedimentology*, **20**, pp. 321–336. Elsevier, Amsterdam.

Serebryakov, S.N. and **Semikhatov, M.A.** (1974) Riphean and recent stromatolites: a comparison. *Am. J. Sci.*, **274**, 556–574.

Sergeev, V.N. (1994) Microfossils in cherts from the Middle Riphean (Mesoproterozoic) Avzyan Formation, southern Ural Mountains, Russian Federation. *Precambrian Res.*, **65**, 231–254.

Sergeev, V.N. (2009) The distribution of microfossil assemblages in Proterozoic rocks. *Precambrian Res.*, **173**, 212–222.

Sheldon, N.D. (2013) Causes and consequences of low atmospheric pCO_2 in the late Mesoproterozoic. *Chem. Geol.*, **362**, 224–231.

Shi, M., **Feng, Q.-L.** and **Zhu, S.-X.** (2014) Biotic evolution and its relation with geological events in the Proterozoic Yanshan Basin, North China. *Sci. China Earth Sci.*, **57**, 903–918.

Shinn, E.A., **Lloyd, R.M.** and **Ginsburg, R.N.** (1969) Anatomy of a modern carbonate tidal-flat., Andros Island, Bahamas. *J. Sed. Petrol.*, **39**, 1202–1228.

Sperling, E.A., **Halverson, G.P.**, **Knoll, A.H.**, **Macdonald, F.A.** and **Johnston, D.T.** (2013) A basin redox transect at the dawn of animal life. *Earth Planet. Sci. Lett.*, **371–372**, 143–155.

Stal, L.J. (1995) Physiological ecology of cyanobacteria in microbial mats and other communities. *New Phytol.*, **131**, 1–32.

Stoodley, P., **Lewandowski, Z.**, **Boyle, J.D.** and **Lappin-Scott, H.M.** (1999) The formation of migratory ripples in a mixed species bacterial biofilm growing in turbulent flow. *Environ. Microbiol.*, **1**, 447–455.

Su, W.B., **Zhang, S.H.**, **Huff, W.D.**, **Li, H.K.**, **Ettensohn, F.R.**, **Chen, X.Y.**, **Yang, H.M.**, **Han, Y.G.**, **Song, B.** and **Santosh, M.** (2008) SHRIMP U-Pb Ages of K-Bentonite Beds in the Xiamaling Formation: Implications for Revised Subdivision of the Meso- to Neoproterozoic History of the North China Craton. *Gondwana Res.*, **14**, 543–553.

Su, W.B., **Li, H.K.**, **Huff, W.D.**, **Ettensohn, F.R.**, **Zhang, S.H.**, **Zhou, H.Y.** and **Wan, Y.S.** (2010) SHRIMP U-Pb dating for a K-bentonite bed in the Tieling Formation, North China. *Chinese Sci. Bull.*, **55**, 2197–2206.

Suárez-González, P., **Quijada, I.E.**, **Benito, M.I.**, **Mas, R.**, **Merinero, R.** and **Riding, R.** (2014) Origin and significance of lamination in Lower Cretaceous stromatolites and proposal for a quantitative approach. *Sed. Geol.*, **300**, 11–27.

Syvitski, J.P.M., **Slingerland, R.L.**, **Burgess, P.**, **Meiburg, E.**, **Murray, A.B.**, **Wiberg, P.**, **Tucker, G.** and **Voinov, A.A.** (2010) Morphodynamic models: an overview. In: *River, coastal, and estuarine morphodynamics* (Ed. C.A. Vionnet), pp. 3–20. Taylor and Francis, Boca Raton.

Teyssèdre, B. (2006) Are the green algae (phylum Viridiplantae) two billion years old? Carnets de Géologie/ Notebooks on Geology - Article 2006/03 (CG2006_A03).

Thomas, K., **Herminghaus, S.**, **Porada, H.** and **Goehring, L.** (2013) Formation of *Kinneyia* via shear-induced instabilities in microbial mats. *Phil. Trans. R Soc. A*, **371**, 20120362.

Thompson, J.B. and **Ferris, F.G.** (1990) Cyanobacterial precipitation of gypsum, calcite, and magnesite from natural alkaline lake water. *Geology*, **18**, 995–998.

Tice, M.M., **Thornton, D.C.O.**, **Pope, M.C.**, **Olszewski, T.D.** and **Gong, J.** (2011) Archean microbial mat communities. *Annu. Rev. Earth Planet. Sci.*, **39**, 297–319.

Tosti, F. and **Riding, R.** (2015) Sinusoidal columnar stromatolites from the Mesoproterozoic of northern China: origin and significance. 2015 GSA Annual Meeting in Baltimore, Maryland, USA (1-4 November 2015), Paper No. 280-5.

Tosti, F. and **Riding, R.** (2017) Current molded, storm damaged, sinuous columnar stromatolites: Mesoproterozoic of northern China. *Palaeogeogr. Palaeoclimatol. Palaeoecol.*, **465**, 93–102.

Trompette, R. (1969) Les stromatolites du 'Précambrien supérieur' de L'Adrar de Mauritanie (Sahara occidental). *Sedimentology*, **13**, 123–154.

Truswell, J.F. and **Eriksson, K.A.** (1973) Stromatolitic associations and their palaeo-environmental significance: a re-appraisal of a lower Proterozoic locality from the Northern Cape Province, South Africa. *Sed. Geol.*, **10**, 1–23.

Vandenbruwaene, W., **Temmerman, S.**, **Bouma, T.J.**, **Klaassen, P.C.**, **De Vries, M.B.**, **Callaghan, D.P.**, **Van Steeg, P.**, **Dekker, F.**, **Van Duren, L.A.**, **Martini, E.** and **Balke, T.** (2011) Flow interaction with dynamic vegetation patches: implications for biogeomorphic evolution of a tidal landscape. *J. Geophys. Res.*, **116**, F01008. doi:10.1029/2010JF001788.

Verbruggen, H., **Ashworth, M.**, **LoDuca, S.T.**, **Vlaeminck, C.**, **Cocquyt, E.**, **Sauvage, T.**, **Zechman, F.W.**, **Littler, D.S.**, **Littler, M.M.**, **Leliaert, F.** and **De Clerck, O.** (2009) A multi-locus time-calibrated phylogeny of the siphonous green algae. *Mol. Phylogenet. Evol.*, **50**, 642–653.

Veselovskiy, R.V., **Pavlov, V.E.** and **Petrov, P.Y.** (2009) New paleomagnetic data on the Anabar Uplift and the Uchur-Maya Region and their implications for the paleogeography and geological correlation of the Riphean of the Siberian Platform, Izvestiya. *Phys. Solid Earth*, **45**, 545–566.

Walcott, C.D. (1906) Algonkian formations of northwestern Montana. *Geol. Soc. Am. Bull.*, **17**, 1–28.

Walcott, C.D. (1910) Abrupt appearance of the Cambrian fauna on the North American continent. *Smithson. Misc. Coll.*, **57**, 1–10.

Walcott, C.D. (1914) Cambrian geology and paleontology III: precambrian Algonkian algal flora. *Smithson. Misc. Coll.*, **64**, 77–156.

Walter, M.R. (1972) Stromatolites and the biostratigraphy of the Australian Precambrian and Cambrian. *Spec. Pap. Palaeontol.*, **11**, 256.

Walter, M.R., **Bauld, J.** and **Brock, T.D.** (1976) Morphology and morphogenesis of columnar stromatolites (Conophyton, Vacerilla) from hot springs in Yellowstone National Park. In: *Stromatolites* (Ed. M.R. Walter), *Dev. Sedimentol.*, 20, pp. 273–310. Elsevier, Amsterdam.

Walter, M.R., **Grotzinger, J.P.** and **Schopf, J.W.** (1992) Proterozoic stromatolites. In: *The Proterozoic biosphere: a multidisciplinary study* (Eds J.W. Schopf and C. Klein), pp. 253–260. Cambridge University Press, Cambridge.

Wang, W., **Liu, S.**, **Santosh, M.**, **Zhang, L.**, **Bai, X.**, **Zhao, Y.**, **Zhang, S.** and **Guo, R.** (2015) 1.23 Ga mafic dykes in the North China Craton and their implications for the reconstruction of the Columbia supercontinent. *Gondwana Res.*, **27**, 1407–1418.

Weerman, E.J., **van de Koppel, J.**, **Eppinga, M.B.**, **Montserrat, F.**, **Liu, Q.-X.** and **Herman, P.M.J.** (2010) Spatial self-organization on intertidal mudflats through biophysical stress divergence. *Am. Nat.*, **176**, E15–E32.

Whale, G.F. and **Walsby, A.E.** (1984) Motility of the cyanobacterium *Microcoleus chthonoplastes* in mud. *Brit. Phycol. J.*, **19**, 117–123.

White, B. (1970) Algal stromatolites, depositional environments and age of the Altyn Formation of Montana. *Geol. Soc. Am.*, Abstracts with Programs, **2**, 719–720.

White, B. (1984) Stromatolites and associated facies in shallowing-upward cycles from the Middle Proterozoic Altyn Formation of Glacier National Park, Montana. *Precambrian Res.*, **24**, 1–26.

Wilde, S.A. (2014) The Precambrian geology of the North China craton: a review and update of the key issues. In: *Evolution of Archean Crust and Early Life* (Eds Y. Dilek and H. Furnes), Modern Approaches Solid Earth Sci., **7**, 149–178.

Winston, D. (1986) Sedimentation and tectonics of the Middle Proterozoic Belt basin and their influence on Phanerozoic compression and extension in western Montana and northern Idaho. In: *Paleotectonics and Sedimentation in the Rocky Mountain Region* (Ed. J.A. Peterson), **41**, pp. 87–118, American Association of Petroleum and Geological Memoirs, USA.

Winston, D. (1990) Evidence for intracratonic, fluvial and lacustrine settings of Middle and Late Proterozoic basins of western USA. In: *Mid-Proterozoic Laurentia–Baltica* (Eds C.F. Gower, T. Rivers and B. Ryan), *Geological Association of Canada Special Paper*, **38**, pp. 536–564. Geological Association of Canada, Canada.

Winston, D. (2007) Revised stratigraphy and depositional history of the Helena and Wallace Formations, Mid-Proterozoic Piegan Group, Belt Supergroup, Montana and Idaho. In: *Proterozoic Geology of Western North America and Siberia* (Eds P.K. Link and R.S. Lewis), SEPM Spec. Publ., **86**, 65–100.

Woosley, R.J., **Millero, F.J.** and **Grosell, M.** (2012) The solubility of fish-produced high magnesium calcite in seawater. *J. Geophys. Res.*, **117**, C0401822.

Young, R.B. (1934) A comparison of certain stromatolitic rocks in the Dolomite Series of South Africa with modern algal sediments in the Bahamas. *Trans. Geol. Soc. S. Afr.*, **37**, 153–162.

Young, G.M. (1974) Stratigraphy, paleocurrents and stromatolites of Hadrynian (upper Precambrian) rocks of Victoria Island, Arctic Archipelago, Canada. *Precambrian Res.*, **1**, 13–41.

Young, G.M. and **Long, D.G.F.** (1976) Stromatolites and basin analysis: an example from the Upper Proterozoic of northwestern Canada. *Palaeogeogr. Palaeoclimatol. Palaeoecol.*, **19**, 303–318.

Zhai, M., **Bian, A.** and **Zhao, T.** (2000) The amalgamation of the supercontinent of North China Craton at the end of Neo-Archaean and its breakup during late Palaeoproterozoic and Meso-Proterozoic. *Sci. China (Series D)*, **43**, 219–232.

Zhang, C.-H., **Li, C.-M.**, **Deng, H.-L.**, **Liu, Y.**, **Liu, L.**, **Wei, B.**, **Li, H.-B.** and **Liu, Z.** (2011) Mesozoic contraction deformation in the Yanshan and northern Taihang mountains and its implications to the destruction of the North China Craton. *Sci. China Earth Sci.*, **54**, 798–822.

Zhang, S., **Li, Z.-X.**, **Evans, D.A.D.**, **Wu, H.**, **Li, H.** and **Dong, J.** (2012) Pre-Rodinia supercontinent Nuna shaping up: a global synthesis with new paleomagnetic results from North China. *Earth Planet. Sci. Lett.*, **353–354**, 145–155.

Zhao, G. (2001) Palaeoproterozoic assembly of the North China Craton. *Geol. Mag.*, **138**, 89–91.

Zhao, G. (2014) *Precambrian evolution of the North China Craton*. Elsevier, Oxford, 194 pp.

Zhao, G. and **Cawood, P.A.** (2012) Precambrian geology of China. *Precambrian Res.*, **222–223**, 13–54.

Zhao, G., **Sun, M.** and **Wilde, S.A.** (2002) Reconstruction of a pre-Rodinia supercontinent: new advances and perspectives. *China Sci. Bull.*, **47**, 1585–1588.

Zhao, G., **Sun, M.**, **Wilde, S.A.** and **Li, S.** (2004) A Paleo-Mesoproterozoic supercontinent: assembly, growth and breakup. *Earth-Sci. Rev.*, **67**, 91–123.

Zhou, X.-Q., **Li, N.**, **Liang, G.-S.**, **Li, L.**, **Tang, D.-J.** and **Fu, X.-M.** (2009) Sedimentary significance of the autochthonous glauconite in stromatolitic limestones of the Mesoproterozoic Tieling Formation in Jixian, Tianjin, North China. *Geol. Bull. China*, **28**, 985–990.

Manuscript received 24 May 2016; revision accepted 14 October 2016